Journal of Visualized Experiments

High-Throughput Measurement of the Plasma Membrane Resealing Efficiency in Mammalian Cells

--Manuscript Draft--

Article Type:	Invited Methods Article - JoVE Produced Video
Manuscript Number:	JoVE58351R2
Full Title:	High-Throughput Measurement of the Plasma Membrane Resealing Efficiency in Mammalian Cells
Keywords:	plasma membrane resealing; membrane repair; muscular dystrophy; propidium iodide; TO-PRO-3; pore-forming toxin; listeriolysin O
Corresponding Author:	Stephanie Seveau Ohio State University Columbus, Ohio UNITED STATES
Corresponding Author's Institution:	Ohio State University
Corresponding Author E-Mail:	Stephanie.Seveau@osumc.edu;seveau.1@osu.edu
Order of Authors:	Jonathan G.T. Lam
	Chi Song
	Stephanie Seveau
Additional Information:	
Question	**Response**
Please indicate whether this article will be Standard Access or Open Access.	Standard Access (US$2,400)
Please indicate the **city, state/province, and country** where this article will be **filmed**. Please do not use abbreviations.	770 Biomedical Research Tower 460 W 12th Avenue Columbus, Ohio 43212

TITLE:

High-Throughput Measurement of Plasma Membrane Resealing Efficiency in Mammalian Cells

AUTHORS & AFFILIATIONS:

Jonathan G.T. Lam[1,2,3], Chi Song[4], and Stephanie Seveau[1,2,3]

[1]Department of Microbial Infection and Immunity, The Ohio State University, Columbus, Ohio, USA
[2]Department of Microbiology, The Ohio State University, Columbus, Ohio, USA
[3]Infectious Diseases Institute, The Ohio State University, Columbus, Ohio, USA
[4]Division of Biostatistics, College of Public Health, The Ohio State University, Columbus, Ohio, USA

Corresponding Author:

Stephanie Seveau (Seveau.1@osu.edu)
Tel: (614) 247-7674

Email Addresses of Co-Authors:

Jonathan G.T. Lam (Lam.215@osu.edu)
Chi Song (Song.1188@osu.edu)

KEYWORDS:

Plasma membrane resealing, membrane repair, muscular dystrophy, propidium iodide, carbocyanine nucleic acid binding dye, pore-forming toxin, listeriolysin O

SUMMARY:

Here we describe a high-throughput fluorescence-based assay that measures the plasma membrane resealing efficiency through fluorometric and imaging analyses in living cells. This assay can be used for screening drugs or target genes that regulate plasma membrane resealing in mammalian cells.

ABSTRACT:

In their physiological environment, mammalian cells are often subjected to mechanical and biochemical stresses that result in the plasma membrane damage. In response to these damages, the plasma membrane is rapidly resealed by complex molecular machinery to restore its barrier function and maintain cell survival. Despite 60 years of research in this field, we still lack a thorough understanding of the cell resealing machinery. With the goal of identifying cellular components that control plasma membrane resealing or drugs that can improve resealing, we have developed a fluorescence-based high-throughput assay that measures the plasma membrane resealing efficiency in mammalian cells cultured in microplates. As a model system for plasma membrane damage, cells are exposed to the bacterial pore-forming toxin listeriolysin O (LLO), which forms large 30-50 nm diameter proteinaceous pores in cholesterol-containing membranes. The use of a temperature-controlled multi-mode microplate reader allows for the rapid and the sensitive spectrofluorometric measurements in combination with brightfield and

fluorescence microscopy imaging of living cells. Kinetic analysis of the fluorescence intensity emitted by a membrane impermeant nucleic acid-binding fluorochrome reflects the extent of membrane wounding and resealing at the cell population level, allowing for the calculation of the cell resealing efficiency. Microscopy imaging allows for enumeration of cells in each well of the microplate to account for potential variations in their number and allows for eventual identification of distinct cell populations. This high-throughput assay is a powerful tool expected to expand our understanding of membrane repair mechanisms via screening for host genes or exogenously added compounds that control plasma membrane resealing.

INTRODUCTION:

Mammalian cells are subject to mechanical, osmotic, and biochemical stress, resulting in the loss of plasma membrane integrity. Without rapid and efficient resealing, damaged cells would quickly succumb to programmed or necrotic death. Since the 1960s, efforts to understand the plasma membrane resealing process have been motivated by the devastating consequences associated with its dysfunctions. Indeed, diseases such as Limb-Girdle Muscular Dystrophy, diabetes, and Chediak-Higashi Syndrome have been linked to deficient plasma membrane repair due to mutations in the gene encoding dysferlin, production of advanced glycation end products, and defects in the lysosomal trafficking regulator CHS1, respectively[1-6]. However, to date, our understanding of membrane resealing is still limited[7]. Initial studies have demonstrated that membrane resealing is initiated by the influx of extracellular Ca^{2+} through a damaged plasma membrane[8-10]. Since then, several non-mutually exclusive Ca^{2+}-dependent mechanisms have been proposed to reseal cells. The patch hypothesis proposes that in proximity to the wound, intracellular vesicles fuse with each other and the damaged plasma membrane to act as a patch[11-14]. A second model proposes that calcium-dependent exocytosis of lysosomes at the wound site releases the lysosomal enzyme acid sphingomyelinase, which converts sphingomyelin to ceramide in the outer leaflet of the plasma membrane. This sudden change in lipid composition results in ceramide-driven endocytosis of the damaged region[15-17]. Lastly, the third proposed mechanism involves a role for the endosomal sorting complex required for transport (ESCRT) to promote the formation of outward-facing vesicles that bud off from the plasma membrane[18]. Only a limited set of proteins was identified in these models, and their machinery must be further elucidated.

Here we describe a high-throughput assay that measures the plasma membrane resealing efficiency in adherent mammalian cells subjected to damage mediated by recombinant listeriolysin O (LLO)[19]. LLO is a pore-forming toxin (PFT) secreted by the facultative intracellular pathogen *Listeria monocytogenes*[20-22] and belongs to the MACPF/CDC (membrane attack complex, perforin, and cholesterol-dependent cytolysin) superfamily. MACPF are mammalian pore-forming proteins involved in immune defenses, whereas CDCs are bacterial toxins mainly produced by gram-positive pathogens that damage host cells to promote pathogenic lifestyles[23]. CDCs are synthesized as water-soluble monomers or dimers that bind to cholesterol present in the plasma membrane and oligomerize into a prepore complex of up to 50 subunits. The prepore complex then rearranges to insert β-strands across the lipid bilayer, forming a β-barrel pore that spans 30-50 nm in diameter[24-27]. These large pores permit fluxes of ions and small cellular components in and out of the cell; though, some studies have proposed that pores of smaller

sizes are also formed[28-30]. Among the CDCs, LLO displays unique properties including irreversible pH- and temperature-dependent aggregation, which is conducive to high-throughput analyses[31,32]. LLO can be added to a cell culture medium at 4 ˚C (a temperature permissive to its binding to cells), but not to the formation of the pore complex. Initiation of pore formation can then be synchronized by raising the temperature to 37 ˚C, allowing for the efficient diffusion of toxin molecules in the plane of the membrane and formation of pore complexes. The time to form pores and the degree of cell damage will therefore depend on the amount of toxin bound to the plasma membrane. Importantly, unbound and soluble LLO can rapidly and irreversibly aggregate when the temperature reaches 37 ˚C, which alleviates the need to wash away unbound toxins and limits the extent of membrane damage over time. Lastly, because LLO binds to cholesterol and forms pores in cholesterol-rich membranes, this assay is amenable to a wide range of mammalian cells. It is important to keep in mind that LLO affects host cell signaling mainly via pore formation, with a few exceptions in which pore-independent cell signaling can occur[33-39]. Therefore, it cannot be excluded that LLO signaling activities may influence the process of membrane repair.

This assay directly assesses the extent of cell wounding by measuring the incorporation of a cell impermeant fluorochrome (*e.g.,* propidium iodide) that passively enters wounded cells and becomes highly fluorescent once it associates with nucleic acids. Hence, the fluorochrome can be maintained in the cell culture medium throughout the experiment, allowing real-time analyses of cell wounding. The fluorescence intensity of the nucleic acid-binding dye will increase with the concentration of toxin and, for a given concentration of toxin, will increase over time until all pores are formed, and cells are fully repaired or until saturation is reached. The influx of extracellular Ca^{2+} through membrane pores is a *sine qua non* event for resealing. Therefore, the resealing efficiency can be indirectly evidenced by comparing cell wounding in culture medium containing Ca^{2+} (repair permissive condition) to wounding in a Ca^{2+}-free medium (repair restrictive condition), allowing for calculation of the resealing efficiency. Because the fluorescence intensity of the nucleic acid-binding dye is directly proportional to the cell concentration in each well, it is important to seed cells at the same concentration in all wells. It is also important to enumerate cells in each well before and after the assay to ensure that no detachment occurs, which may complicate data interpretation. To enumerate cells, cells expressing nuclear-localized histone 2B-GFP (H2B-GFP) were used in this assay. Temperature-controlled, multi-mode, microplate readers combine rapid, high-throughput measurements (using a 96 or 384-well plate format) of fluorescence intensities with microscopy imaging of living cells at 37 °C. The latter can be used to enumerate cell number and observe the eventual formation of distinct cell populations.

Ultimately, this assay provides users the ability to expand their knowledge of the complexity of membrane repair mechanisms by screening for host molecules or exogenously added compounds that control membrane repair. The following protocol describes the experimental steps to measure the resealing efficiency of cells exposed to LLO and evaluate the effects of a given drug or cellular treatment on resealing efficiency.

PROTOCOL:

1. Preparation

1.1 Cell Plating

Note: Human cervical epithelial cells, HeLa and HeLa expressing Histone 2B-GFP (H2B-GFP), were used in this protocol, but this assay can be adapted to other mammalian cells[19].

1.1.1 Detach adherent cells from a 75 cm^2 cell culture flask by washing the cells with 2 mL of Trypsin-EDTA 0.25%. Replace the used trypsin with 2 mL of fresh trypsin-EDTA 0.25%.

1.1.2 Incubate the cells at 37 ˚C for 5 min until the cells have rounded and detached from the flask.

1.1.3 Resuspend the cells in 8 mL of growth medium (DMEM containing 10% heat-inactivated fetal bovine serum, 100 U/mL penicillin, and 100 µg/mL streptomycin).

1.1.4 Determine the cell concentration using a hemocytometer and 10 µL of cell suspension.

1.1.5 Dilute the cells in growth medium to a concentration of 2.5 x 10^5 cells/mL.

1.1.6 Pour the cell suspension into a sterile pipette basin and thoroughly mix the suspension using a 10 mL serological pipette.

1.1.7 Using a 12-multichannel micropipette and 200 µL tips, distribute HeLa cells (2.5 x 10^4 cells/100 µL/well) in triplicate (or quadruplicate) in a 96-well flat, clear bottom, black polystyrene tissue culture-treated plate.

Note: A plating arrangement is presented as an example in **Figure 1**.

1.1.8 Culture the cells for 24 h in a humidified cell culture incubator at 37 ˚C and 5% CO_2.

1.2 Stock Solution Preparation

1.2.1 Prepare 1 L of a 10x stock of buffer M (used to prepare M1 and M2) by adding 1) 95 g of Hanks Balanced Salt Solution, 2) 0.476 g of $MgCl_2$ (5 mM), and 3) 23.83 g of HEPES (100 mM) to 900 mL of water. Adjust the pH to 7.4 and raise the volume to 1 L. Filter sterilize.

1.2.2 Prepare 50 mL of a 50x (1.25 M) stock of glucose by adding 11.26 g of D-(+)-Glucose to a total of 50 mL of water. Filter sterilize the solution.

1.2.3 Prepare 50 mL of a 100x (120 mM) stock of calcium by adding 0.666 g of $CaCl_2$ to a total of 50 mL of water. Filter sterilize the solution.

1.2.4 Prepare 50 mL of a 10x (50 mM) stock of ethylene glycol-bis(2-aminoethylether)-N,N,N',N',tetraacetic acid (EGTA) by adding 0.951 g of EGTA to 40 mL of water. Increase the pH to 8 using NaOH to dissolve the EGTA, then raise the volume to 50 mL. Filter sterilize the solution.

1.2.5 For a single 96-well plate, prepare 50 mL of Medium 1 (M1, contains Ca^{2+}), 50 mL of Medium 2 (M2, Ca^{2+}-free), and 15 mL of Medium 2 supplemented with EGTA, accordingly:

1.2.5.1 For M1, add 5 mL of 10x Buffer M, 0.5 mL of 100x $CaCl_2$, and 1 mL of 50x glucose to 43.5 mL of water.

1.2.5.2 For M2, add 5 mL of 10x Buffer M and 1 mL of 50x glucose to 44 mL of water.

1.2.5.3 For M2/EGTA, add 1.5 mL of 10x Buffer M and 1.5 mL of 10x EGTA to 12 mL of water.

Note: All solutions containing propidium iodide (PI) should be prepared directly prior to adding to the cells.

1.3 Plate Reader/Imaging Cytometer Settings

Note: Use a multi-mode plate reader equipped with two detection units: a spectrofluorometer and an imaging cytometer. Limit the fluorescence exposure to avoid photobleaching the fluorophores.

1.3.1 Pre-warm the plate reader to 37 °C before performing the assay.

1.3.2 Set up the parameters for the kinetic assay accordingly within the **Settings** mode:

1.3.2.1 Choose **Monochromator**, **FL (fluorescence)**, and **Kinetic** for the optical configuration, read modes, and read type, respectively.

1.3.2.2 Under **Wavelength Settings**, select a 9 and 15 nm excitation and emission bandpass, respectively. For assays using propidium iodide (PI), set the excitation and emission wavelengths to 535 and 617 nm, respectively.

1.3.2.3 Under **Plate Type**, select **96 Wells** for the plate format and a pre-set plate configuration corresponding to a black-wall clear bottom plate.

1.3.2.4 Under **Read Area**, highlight the wells that will be analyzed throughout the kinetic.

1.3.2.5 Under **PMT and Optics**, preset the flashes per read to **6** and check the box for **Read from Bottom**.

1.3.2.6 Under **Timing**, insert **00:30:00** in the **Total Run Time** box for a 30 min kinetic assay, and insert **00:05:00** for the **Interval**.

Note: For each time point and one wavelength, the reading time of a full 96-well plate is 30 s.

1.3.2.7 Confirm the specified settings in the **Settings Information** to the right and select **OK**. Press **Read** to initiate the kinetic run.

1.3.3 Set up the imaging parameters accordingly within the Settings mode:

1.3.3.1 Choose **Minimax**, **Imaging**, and **Endpoint** for the optical configuration, read modes, and read type, respectively.

1.3.3.2 Under **Wavelengths**, select **transmitted light**, and either or both the fluorescence boxes corresponding to excitation and emission wavelengths of 456/541 nm (GFP) and 625/713 nm (PI).

1.3.3.3 Use the same options for the **Plate Type** and **Read Area** as defined in steps 1.3.2.3 and 1.3.2.4.

1.3.3.4 Under **Well Area Setting**, select the number of sites within a well to be imaged.

Note: 12 sites correspond to a full-well image.

1.3.3.5 Under the **Image Acquisition Settings**, select the exposure times for transmitted light: 541 (GFP), and 713 (PI). For GFP, image the entire well with an exposure time of 20 ms/image. For transmitted light (TL) and PI fluorescence, acquire a single image of the center of each well with exposure times of 8 and 20 ms, respectively.

1.3.3.6 Confirm the specified settings in the **Settings** Information to the right and select **OK**. The acquisition time for imaging the entire surface of each well (12 images/well) of a 96-well plate and for one wavelength is ~15 min/plate. Press **Read** to initiate imaging.

Note: The acquisition time of a single image/well of a 96-well plate requires ~2.5 min/plate for one wavelength. The parameters described above correspond to the specific equipment in our laboratory. Spectrofluorometric measurements: A xenon flash lamp displaying 1.0 nm increment excitation wavelengths (250-850 nm) with an adjustable 9 or 15 nm bandpass, a photomultiplier tube detector with a > 6 log dynamic range and an adjustable 15 or 25 nm emission bandpass. Imaging cytometer: An illumination light source capable of white light, 460 nm and 625 nm excitation wavelengths with a 20 nm bandpass, emission filters centered at 541 nm (108 nm bandpass) and 713 nm (123 nm bandpass), respectively, and a 4X objective coupled to a 1.25 megapixel 12-bit charge-coupled device camera.

2. Assay

Note: At the time of the assay, cells must be 70-90% confluent. During the wash steps, the medium should be removed from and applied to the side-wall of the well (not directly above the

cells). Maintain the temperature of LLO at < 4 ˚C to prevent its aggregation until step 3.1.5.

2.1.1 Prepare a stock of 30 µM PI in M1 and a stock of 30 µM PI in M2 pre-warmed at 37 ˚C.

2.1.2 Gently wash the cells in plate 1 using a 12-multichannel micropipette and 200 µL tips, as follows:

2.1.2.1 For repair-permissive conditions, remove the growth medium and wash the cells twice with 200 µL/well M1 pre-warmed at 37 ˚C. Replace the medium with 100 µL/well of warm M1 containing 30 µM PI.

2.1.2.2 For repair restrictive-conditions, remove the growth medium and wash the cells once with 200 µL/well warm M2 containing 5 mM EGTA to chelate Ca^{2+}, followed by one wash with 200 µL/well M2. Replace the medium with 100 µL/well warm M2 containing 30 µM PI.

2.1.2.3 After the growth medium has been washed and replaced with medium containing propidium iodide, directly move to step 2.1.3.

2.1.3 Image plate 1 under transmitted light, GFP, and PI as detailed under 1.3.3 (pre-kinetic). This step takes 15-20 min.

2.1.4 During the 15 min period in step 2.1.3, prepare plate 2 using a 12-multichannel micropipette and 200 µL tips as follows:

2.1.4.1 Place a 96-well round bottom polypropylene microplate on ice. Configure the plate using an experimental design corresponding to plate 1 (**Figure 1**).

2.1.4.2 For repair-permissive conditions, add 100 µL/well of ice-cold M1 containing 60 µM PI, followed by the addition of 100 µL/well of ice-cold M1 containing 4x LLO or not for the control.

2.1.4.3 For repair-restrictive conditions, add 100 µL/well of ice-cold M2 containing 60 µM PI, followed by the addition of 100 µL/well of ice-cold M2 containing 4x LLO or not for the control.

2.1.5 After imaging plate 1 (step 2.1.3), immediately place it on ice, using aluminum foil to separate the plate from direct contact with ice. Allow plate 1 to cool down for 5 min.

2.1.6 Using a 12-multichannel micropipette and 200 µL tips, transfer 100 µL from each well into plate 2 (step 3.1.1) to the corresponding wells in the plate 1. To properly distribute the toxin in the media, insert the tips below this meniscus and gently eject the volume without introducing bubbles.

Note: Do not pipette up and down, as this may inadvertently detach the cells.

2.1.7 Leave the plate for an additional 1 min to allow the toxin to bind to host cells and

immediately transfer plate 1 to the plate reader for the kinetic assay using the spectrofluorometer mode (step 1.3.2).

2.1.8 At the end of the kinetic assay, immediately image plate 1 (post-kinetic) using step 1.3.3.

3 Analysis: Cell Enumeration

3.1. Determine the cell count based on the nuclear fluorescence using the microplate cell enumeration software.

3.1.1 Within **Settings,** select **Re-analysis**, and under the category section within the **Image Analysis Settings** select **Discreet Object Analysis** using **541** as the wavelength for finding objects.

3.1.2 Within the Find Objects option, using the **Draw on Images** finding method, select **Nuclei** under the settings tab, and press **Apply**.

3.1.3 Press **OK** and **Read** to initiate the cell counting algorithm.

3. Alternatively, if no such tool is available, use an image analysis software such as ImageJ to enumerate cells.

3.2.1 In ImageJ, open the image file as a stack.

3.2.2 Convert the stack to 8-bit greyscale images by clicking **Image** in the menu bar, hover over **Type,** and select **8-bit**.

3.2.3 Subtract the background: Click **Image** in the menu bar, hover over **Adjust**, and select **Brightness/Contrast**. Adjust the minimum value to remove the background noise and select **Apply**.

3.2.4 Threshold to create binary images: Click **Image** in the menu bar, hover over **Adjust**, and select **Threshold**. Select **Dark background**, adjust the minimum and maximum threshold values, and click **Apply**.

3.2.5 In the case of overlapping nuclei, a Watershed tool can be used to segment nuclei. Click **Process** in the menu, hover over **Binary** and select **Watershed**.

Note: This will automatically separate connected nuclei.

3.2.6 Analyze the masked images by applying user-specified criteria (size and circularity) to refine the identification of nuclei and exclude cell debris.

3.2.6.1 Click on **Analyze** in the menu and then **Analyze particles**. Set the desired size (pixel^2) and circularity (a value of 1 is a perfect circle) ranges that are sufficient to include individual

cells/nuclei.

3.2.6.2 In the Show dropdown box, select the option(s) desired, check **Summarize**, and click **OK** to obtain cell counts.

4. Analysis: Kinetic Curves

4.1. Transfer the kinetic data from the plate reader software to an analytical data software.

4.2. For each experimental condition, average the fluorescence intensities of the replicates at each timepoint, along with the corresponding standard deviation and standard error of the mean for each experimental condition.

4.3. For each experimental condition, trace the corresponding kinetic curve: PI intensity (y-axis) versus time (x-axis).

4.4. To calculate the resealing efficiency of a given treatment condition, calculate the area under the curve (AUC) of the +LLO in M1 (AUC(M1)) and +LLO in M2 (AUC(M2)). Use the approach suggested below to assess the efficiency (E) of resealing:

$$4\mathrm{E} = 1 - \left[\frac{\mathrm{AUC(M1)}}{\mathrm{AUC(M2)}}\right] = \frac{\mathrm{AUC(M2)} - \mathrm{AUC(M1)}}{\mathrm{AUC(M2)}}$$

4.5. Perform a comparison between control and test treatment by determining the efficiency ratio (R_{Eff}) indicated below:

3.2.6.3 $$\mathrm{R_{EFF}} = \frac{\mathrm{Etest}}{\mathrm{Econtrol}} = \frac{\mathrm{AUC(control,\ M2)}}{\mathrm{AUC(test,\ M2)}} * \left[\frac{\mathrm{AUC(test,\ M2) - AUC(test,\ M1)}}{\mathrm{AUC(control,\ M2) - AUC(control,\ M1)}}\right]$$

$\mathrm{R_{EFF}} = 1$, test treatment has no effect on repair
$\mathrm{R_{EFF}} < 1$, test treatment inhibits repair
$\mathrm{R_{EFF}} > 1$, test treatment improves repair

4.6. Calculate the area under the curve using the following equation:
$\mathrm{AUC} = \sum_{i=1}^{k-1}(\mathrm{Intensity_{i+1}} + \mathrm{Intensity_i}) \times (\mathrm{Time_{i+1}} - \mathrm{Time_i})/2$, where k is the total number of follow-ups.

REPRESENTATIVE RESULTS:

Cell counting accuracy: HeLa cells are frequently used as a model mammalian cell line to explore membrane repair mechanisms. When assessing membrane repair at the cell population level, it is important to plate cells at the same concentration in all wells for proper data interpretation. It is also important to verify at the time of the assay that cell numbers are equivalent across wells. HeLa cells that constitutively express histone 2B fused to GFP (H2B-GFP) were introduced in this assay to automatically enumerate cells based upon detection of their fluorescent nuclei. To

establish the accuracy in cell enumeration, twofold serial dilutions of HeLa H2B-GFP cells were plated in triplicate in a 96-well plate and cultured for 4 h. This amount of time is sufficient for cell attachment and provides limited cell division. Full wells were imaged under transmitted light (TL) and GFP fluorescence illuminations and cell counts were assessed based on GFP fluorescence using the plate reader analysis software (**Figures 2A** and **2B**). The average cell counts ± standard deviation was plotted against cell seeding concentrations, and a line of best fit indicated a 1.08:1 ratio of cell count to cell seeding, demonstrating the accuracy of the counting (**Figure 2C**). By imaging all of the wells prior to a kinetic assay, it can be ensured that cell numbers are consistent among all wells. Also, by imaging wells after the kinetic assay, one can establish if exposure to the toxin caused cell detachment. This information is critical for accurate interpretation of the kinetic data.

Expression of GFP does not interfere with propidium iodide (PI) intensity measurements (I_{PI}): to ensure that H2B-GFP nuclear association does not interfere with PI incorporation or PI fluorescence intensity measurement (I_{PI}), I_{PI} was compared in HeLa and HeLa H2B-GFP cells that were exposed, or not, to 1 nM LLO (**Figure 3**). In the absence of PI, there was a similarly low level of background fluorescence in HeLa and HeLa H2B-GFP, indicating that GFP does not bleed through PI fluorescence emission filters. In the presence of PI but absence of LLO, there was a similar basal PI fluorescence emission in both HeLa and HeLa H2B-GFP that did not change over time. This confirmed that expression of GFP does not affect measurement of PI fluorescence and indicated that PI does not penetrate non-damaged cells over the time frame of the experiment. Addition of LLO resulted in an increase in PI fluorescence over time that was similar in both HeLa and HeLa H2B-GFP. This increase is due to cell wounding by LLO combined with PI association with nucleic acids. Together, these results establish that expression of Histone-2B-GFP does not affect PI incorporation or measurement of its fluorescence.

PI fluorescence does not interfere with GFP-based cell counting: reciprocally, it was important to verify that PI nuclear incorporation in wounded cells does not interfere with GFP-based cell counting. Representative fluorescence images of HeLa and HeLa H2B-GFP exposed to 1 nM LLO in the presence of PI, showed that there was a marked accumulation of PI in wounded cells post kinetics, as expected (**Figure 4A**). Imaging also revealed that PI could bleed through GFP fluorescence detection (**Figure 4A** and **Table 1**). This fluorescence crossover was best appreciated on the post-kinetic images of HeLa cells that do not express GFP, but it still displayed green fluorescent nuclei (**Figure 4A**). This crossover could also be evidenced by the measurement of GFP fluorescence intensity (I_{GFP}) in HeLa H2B-GFP cells, which significantly increased post-kinetic compared to pre-kinetic (**Figure 4B**). Importantly, PI fluorescence crossover does not affect cell counting because the segmentation process involved in the enumeration of nuclei is unaffected by an increase in GFP fluorescence (**Figure 4C**).

Measuring plasma membrane resealing efficiency: in this section, we present the basic methodology used to measure the efficiency of membrane resealing. To evidence the process of membrane resealing, HeLa H2B-GFP cells were exposed, or not, to 1 nM LLO in the presence (M1) or absence (M2) of extracellular calcium (**Figure 5**). As expected, in the absence of LLO, I_{PI} remained constant in M1 and M2. Addition of LLO in Ca^{2+}-containing medium resulted in a steady

increase in PI fluorescence intensity (I_{PI}), whereas in the absence of extracellular calcium, there was a significantly steeper increase in PI fluorescence, reflecting the absence of membrane resealing. To assess the resealing efficiency, which is defined as the capacity of cells to repair in M1 relative to M2 (step 1.5.4.1), the area under the M1 and M2 curves (AUC) were determined and the efficiency of repair (E) was calculated to be 0.287.

An alternative to PI: PI has been ubiquitously used as a marker for plasma membrane damage. However, there are other nucleic acid binding dyes that are also suitable for this assay. For example, a membrane impermeant carbocyanine nucleic acid binding dye (CNABD) exhibits an emission spectrum reaching into the far red and has a high specificity for double stranded DNA. PI on the other hand binds both DNA and RNA[40,41]. Unlike PI, the excitation and emission spectra of CNABD does not overlap with those of GFP allowing for better spectral resolution between the two fluorochromes. Furthermore, the CNABD used in this protocol has an extinction coefficient nearly twice that of PI, which means that for their respective excitation wavelengths, this dye is more capable of absorbing energy than PI resulting in a stronger fluorescence emission. Quantitative fluorescence analysis of CNABD and GFP images showed that this dye exhibits a large fluorescence dynamic range, does not significantly affect GFP fluorescence, and does not affect cell count (**Figures 6A-D**). Indeed, HeLa H2B-GFP cells incubated in M1 or M2 media containing CNABD and damaged by 1 nM LLO exhibited a 4- and 5.5-fold increase in I_{CNABD} relative to the non-damaged controls, respectively (**Figure 7A**). For comparison, cells exposed to 1 nM LLO in the presence of PI exhibited a 2.5- and 3-fold increase in PI fluorescence intensity in M1 and M2, respectively (**Figure 5**). Like PI, CNABD exhibits increasing fluorescence intensity with increasing LLO concentration in M1 (**Figure 7A**), and the resulting repair efficiency was calculated as described in step 1.5.4.1 (**Figure 7B**). We report that the cell resealing efficiency decreases as LLO concentration increases. This phenomenon reflects the fact that cells decrease their capacity to reseal when excessive damages are caused.

Quality assessment of the membrane repair assay: a critical aspect of any assay is its robustness or capability to detect and resolve differences between the negative and positive controls. Signal variation between positive and negative controls must display sufficient dynamic range and reproducibility. In this membrane repair assay, the negative and positive controls are cells exposed to LLO in repair-permissive (M1) and repair-restrictive (M2) conditions, respectively. Two approaches were taken to assess the robustness of this assay for high-throughput analysis. First, the Z-factor, or screening window coefficient, determines whether a given set of conditions provides a large enough dynamic range, while accounting for signal variability. Z-factors within the ranges $0 < Z \leq 0.5$ and $0.5 < Z \leq 1$ correspond to an acceptable and very good assay, respectively[42,43]. A limitation of using the Z-factor for quality assessment is that tested conditions typically exhibit more moderate values compared to the extreme positive and negative controls. Therefore, as a second approach, we calculated the strictly standardized mean difference (SSMD, β), which can identify differences between experimental conditions that would otherwise be categorized as a negative result based on a qualified Z-factor[44,45]. SSMD values can be categorized into effect strength ranging from no effect ($\beta = 0$) to extremely strong ($\beta \geq 5$). Using the data from **Figure 7A** and AUC for comparison of M1 versus M2 conditions, exposure to 0.25 and 0.5 nM LLO produced Z-factor values of 0.3100813 and 0.137313, and $\beta = 6.0672$ and 4.803308, respectively,

indicating that a window of LLO concentrations is suitable for the assay. As the concentration of LLO is increased beyond 1 nM, the gap in the I_{CNABD} kinetic curves between M1 and M2 conditions closes resulting in drastically reduced Z-factor and SSMD values (**Figure 7B**). Such high concentrations of LLO correspond to conditions in which the repair potential is outweighed by damage and thus negates the use of the assay in identifying factors involved in membrane repair. This is further illustrated by the decrease in repair efficiency (E) as LLO concentration increases (**Figure 7B**). All data (Z-factor, SSMD, and E) were generated with 3 biological replicates and 3 technical replicates per experimental condition for assay validation. Together, these data show that this assay has the expected robustness for a high-throughput assay with LLO concentrations inferior to 1 nM for HeLa cells.

Proof of principle: once the robustness of the assay was established, we performed additional experiments as a proof of principle that this assay has the sensitivity and resolution to identify a defect in the repair process. Also, we considered that high-throughput assays are used as a screening process to identify "hits" within large screens, which may involve less than 3 biological replicates. Thus, it is pertinent that the experimental design provides the detection power to identify "hits" within a single assay. Therefore, under a high-throughput screen, the assay layout can be adjusted to accommodate 4 technical replicates to increase statistical power in a single biological replicate. Cells were plated in quadruplicate and were pre-treated 1 h prior to the assay with desipramine, a pharmacological inhibitor of the lysosomal protein acid sphingomyelinase (ASM) that plays a role in plasma membrane repair[15,17,46]. Importantly, treatment with desipramine did not affect cell counts throughout the assay, allowing for appropriate comparison between desipramine-treated and non-treated cells (**Figure 8A**). Inhibition of ASM in desipramine-treated cells resulted in a defect in membrane resealing efficiency upon exposure to LLO, as illustrated by the decrease in E and R_{Eff} (**Figures 8B** and **8C**). Using a mixed effects model, a comparison of desipramine-treated to non-treated cells in M1 showed p-values of 0.0010 and 1×10^{-10}, respectively. Together, data indicate that 0.25 and 0.5 nM LLO are appropriate concentrations to identify defects in repair in a high-throughput experimental setting, with possible statistical analyses of a single experiment once the technical replicates are increased to four. Note that the statistical approach of the mixed effects model between quadruplicate will not account for potential variations across multiple biological replicates. Any significant findings using one biological replicate should be verified in additional experimental settings.

FIGURE LEGENDS:

Figure 1: Experimental design. The flow diagram depicts a representative plate design configured to test the effect of seven test conditions in comparison to control non-treated cells. Additional controls should be included if appropriate, as for example drug vehicles. Cells are plated (plate 1) 24 h prior to the experiment. On the day of the experiment, cells in plate 1 are washed with M1 or M2 medium pre-warmed at 37 ˚C, and the plate is imaged (TL, GFP and PI fluorescence) pre-kinetic. During the 15 min of imaging, reagents are added on ice to plate 2. After imaging, plate 1 is immediately placed on ice for 5 min, and 100 µL/well are transferred from plate 2 to plate 1. Plate 1 is placed in the plate reader to run the kinetic assay at 37 ˚C for 30 min, followed by imaging (TL, GFP, and PI fluorescence). Data are then analyzed to count cells and assess repair

efficiency in all experimental conditions. In large data sets, analysis can be automated. Also, the number of technical replicates can be increased to 4 in high-throughput screens.

Figure 2: Cell counting accuracy. HeLa cells expressing GFP-tagged Histone 2B were seeded in triplicates at the indicated concentrations. (A) Cells were imaged at 37 ˚C under transmitted light (TL) and GFP fluorescence (12 images/well) and a cell detection algorithm was used to delineate individual nuclei (in purple). Scale bar = 1 mm. (B) Higher magnification of TL, GFP, and cell detection (purple) images (zoomed 2X). Scale bar = 100 µm. (C) Image analysis software was used to count the number of cells and the cell counts were plotted against the initial cell seeding concentration.

Figure 3: Propidium iodide fluorescence measurement is not affected by Histone 2B-GFP expression. Histone 2B-GFP expressing and non-expressing HeLa cells were exposed, or not, to 1 nM LLO in the presence (solid lines) or absence (dashed lines) of 30 µM PI in Ca^{2+}-containing medium (M1). The kinetic assay measured PI fluorescence intensities by spectrofluorometry every 5 min for 30 min at 37 ˚C. Data are the average PI fluorescence intensity (I_{PI}) expressed in relative fluorescence units (RFU) ± SEM (n = 3 independent experiments, each performed in triplicates).

Figure 4: Cell enumeration is unaffected by PI fluorescence. (A) Representative pre- and post-kinetic images (TL, PI, and GFP) of cells exposed, or not, to 1 nM LLO in M1. Scale bar = 100 µm. (B) Quantitative fluorescence microscopy analysis (I_{GFP} ± SEM) revealed the increased GFP fluorescence measurement due to PI nuclear incorporation upon cell wounding by LLO (post-kinetic). (C) GFP-based cell enumeration was unaffected by the increase in GFP intensity. Cell count per well was expressed as average ± SEM. (In B and C: black bars = pre-kinetic data; red bars = post-kinetic data; n = 3 independent experiments, each performed in triplicates; a two-tailed Student's t-test was used to analyze quantitative fluorescence intensity and cell counts from acquired images, **$p < 0.01$).

Figure 5: Measuring plasma membrane resealing efficiency. Histone 2B-GFP expressing HeLa cells were exposed, or not, to 1 nM LLO in Ca^{2+}-containing (M1) or Ca^{2+}-free (M2) medium containing 30 µM PI. Kinetic data represent PI fluorescence intensity (I_{PI}) in relative fluorescence units (RFU) ± SEM, measured for 30 min at 37 ˚C. n = 3 independent experiments, each performed in triplicates. The resealing efficiency was measured as indicated in protocol step 1.5.4.

Figure 6: Carbocyanine nucleic acid binding dye as an alternative dye to assess membrane resealing. HeLa H2B-GFP cells were exposed, or not, to 0.5 nM LLO for 30 min at 37 ˚C in the presence of 1 µM CNABD in Ca^{2+}-containing (M1) or Ca^{2+}-free (M2) medium. (A) Images of HeLa H2B-GFP cells were acquired pre- and post-kinetic in M1 containing the dye. Scale bar = 100 µm. (B and C) Integrated CNABD and GFP fluorescence intensities were measured using the imaging cytometer and expressed in relative fluorescence units (RFU) ± SEM. (D) GFP fluorescence images were processed to enumerate HeLa H2B-GFP cells (black bars = pre-kinetic data, red bars = post-kinetic data, n = 3 independent experiments, each performed in triplicates). A two-tailed Student's t-test was used to analyze quantitative fluorescence intensity and cell counts from

acquired images, **p < 0.01, ***p < 0.001)

Figure 7: Effect of LLO concentration on resealing efficiency, Z-factor, and SSMD. (A) HeLa H2B-GFP cells incubated in M1 or M2 containing 1 µM CNABD were exposed to increasing concentrations of LLO and subjected to the kinetic assay for 30 min at 37 ˚C. Data are expressed as CNABD intensity (I_{CNABD}) in relative fluorescence units (RFU) ± SEM. (B) The Z-factor and strictly standardized mean difference (SSMD) were calculated as a quality assessment for the robustness of the membrane repair assay, using the area under the curve (AUC) as a metric for the kinetic curves[42-45]. The resealing efficiencies were calculated as described in the protocol and results sections (n = 3 independent experiments, each performed in triplicates).

Figure 8: Cell exposure to desipramine causes defects in resealing. HeLa H2B-GFP cells (plated in quadruplicate) were pre-treated with 30 µM desipramine (or not) for 1 h at 37 ˚C and then exposed to 0.25 or 0.5 nM LLO in the presence of 1 µM CNABD in Ca^{2+}-containing (M1) or Ca^{2+}-free (M2) medium. Cells were imaged (pre- and post-kinetic) and subjected to the kinetic assay at 37 ˚C for 30 min. (A) Cells were enumerated; data are expressed as average cell counts ± SEM. (B) CNABD fluorescence intensity (I_{CNABD}) is expressed in relative fluorescence units (RFU) ± SEM. (C) Resealing efficiencies were calculated in the presence and absence of desipramine. A mixed effects model was used on log-transformed intensity values assuming a random intercept for each technical replicate. To capture both a shift and change in shape of the kinetic curves, the main effect of treatment condition and the interaction effect between treatment condition and time were jointly tested for statistical significance. A two-tailed Student's t-test was used to analyze cell counts from acquired images. The p-value was calculated using the mixed effects model. (4 technical replicates, one experiment).

Table 1: GFP, PI, and CNABD excitation and emission peaks and the green and red channel excitation and emission bandpasses for the imaging cytometer.

DISCUSSION:

This assay measures the efficiency of membrane resealing at the cell population level with high-throughput capacity. It can be used to screen for cellular components or drug libraries that could affect membrane repair. The described assay used a 96-well plate format, but it can be adapted to 384-well plates for higher throughput. An advantage of this assay is its ability to obtain fluorescence measurements of adherent living cells in real time without the need for excessive cell processing such as cell detachment, fixation, or fluorescence labeling post-fixation. Multimode plate readers, such as the one used in this protocol, have sufficient sensitivity for rapid spectrofluorometric measurements at time intervals as low as 30 s (for a 96-well plate). The acquisition of fluorescence images provides additional information including cell enumeration and eventual changes in cell morphology, and allows for potential identification of distinct cell populations. The present assay does not claim to establish the kinetics of plasma membrane resealing per se, but does claim to identify experimental conditions (pharmacological compounds or cellular components) that can affect the process of membrane resealing, positively or negatively, within a high-throughput assay.

Several other experimental approaches have been developed to assess the membrane resealing mechanisms. For example, mechanical disruption by needle puncture, bead abrasion, and laser ablation have been used to model membrane damage due to mechanical stress. The measurement of wounding/repair has involved fluorescence microscopy or flow cytometry by quantifying the entry of fluorescent probes (FM 1-43, propidium iodide, fluorescein-conjugated dextrans) or tracking fluorescent protein chimeras[47-50]. Each of these approaches has its own advantages; however, they are not amenable to high-throughput screening in living cells as presented in this assay.

The present assay was optimized to analyze the resealing efficiency of cells wounded by the pore-forming protein LLO, which forms large pores that permit the massive Ca^{2+}influx provoked by mechanical ruptures of the plasma membrane. Although pore-forming toxins represent one form of plasma membrane damage, repair of large toxin pores and mechanical wounds were proposed to share common Ca^{2+}-dependent pathways[17,51]. It is important to note that LLO interaction with cell membrane components such as cholesterol may affect cell signaling and thereby may influence membrane resealing mechanisms when compared to mechanical wounds. Our knowledge about membrane repair is still limited and further studies are required to establish if resealing of mechanical wounds differ from resealing following the formation of toxin pores. There are several advantages of using LLO. First, the initiation of membrane damage can be synchronized by raising the temperature from 4 to 37 ˚C, allowing for multiple conditions to be tested at the same time. Second, the soluble form of LLO (not bound to the cell membrane) irreversibly aggregates at neutral pH and 37 ˚C, thus limiting cytotoxic effects and abrogating the need to wash the cells. Finally, the degree of damage can be adjusted by varying the concentration of the toxin. However, a limitation of this assay is the temperature switch between 37 and 4 ˚C, which may affect the repair mechanism as vesicular transport and membrane fluidity, among other processes, are influenced by temperature[52-54]. It is important to verify that any pharmacological inhibitor included in the assay does not interfere with the formation of LLO pores by performing a hemolysis assay in the presence of the drug[55]. Due to potential batch differences in LLO activity, it is important to prepare a stock of LLO that is large enough for the entire high-throughput screen[55].

We included the use of cells expressing the nuclear-localized Histone-2B-GFP chimera as a means to enumerate cells before and after the membrane repair assay via microscopic imaging followed by automated image analysis. Importantly, equivalent cell counts across conditions and unchanging cell counts before and after the kinetic assay are crucial as PI or CNABD fluorescence intensities cannot simply be normalized. Indeed, a difference in cell count will result in differences in the degree of damage by a given concentration of LLO, which cannot be corrected for via fluorescence normalization due to variations in resealing efficiency (**Figure 7**). We showed that Histone-2B-GFP expression does not interfere with PI or CNABD incorporation or fluorescence emission. Conversely, PI or CNABD incorporation does not affect GFP-based cell enumeration. If other combinations of fluorophores are to be used, it would be necessary to assess potential spectral overlap between fluorochromes, as was performed in this work. Although PI has been extensively used to measure membrane damage, we show that CNABD is an excellent substitute that exhibits higher fluorescence quantum yield, resulting in a larger

dynamic range suitable for characterizing resealing efficiency.

Z-factor and SSMD confirmed that this assay has the robustness necessary to perform high-throughput analyses. The calculation of the resealing efficiency is a critical and reliable tool to identify potential hits. In addition, the mixed effects model can be used as a statistical tool to evaluate hits within a single assay. The experimental plan must include a minimum of three technical replicates if the screen can be repeated several times. Quadruplicates should be used if statistical tools, such as the mixed effects model, are to be included in a single experiment, whether or not it will be repeated. It is advised to perform the screen several times, and it is required to validate the results by performing complementary experiments.

ACKNOWLEDGMENTS:

We acknowledge Dr. Jesse Kwiek (The Ohio State University) for kindly allowing us to use his multi-mode detection platform for some preliminary experiments. Research reported in this article was supported by the National Institute of Allergy and Infectious Diseases of the National Institutes of Health under award number RO1AI107250 to Stephanie Seveau. The content is solely the responsibility of the authors and does not necessarily represent the official views of the National Institutes of Health.

DISCLOSURES:

The authors have nothing to disclose.

REFERENCES:

1. Demonbreun, A.R., E.M. McNally. Plasma Membrane Repair in Health and Disease. *Current Topics in Membranes*. **77**, 67-96 (2016).
2. Howard, A.C., McNeil, A.K., McNeil, P.L. Promotion of plasma membrane repair by vitamin E. *Nature Communications*. **2**, 597 (2011).
3. Howard, A.C., et al. A novel cellular defect in diabetes: membrane repair failure. *Diabetes*. **60** (11), 3034-43 (2011).
4. Lozano, M.L., et al. Towards the targeted management of Chediak-Higashi syndrome. *Orphanet Journal of Rare Diseases*. **9**, 132 (2014).
5. Vainzof, M., et al. Dysferlin protein analysis in limb-girdle muscular dystrophies. *Journal of Molecular Neuroscience*. **17** (1), 71-80 (2001).
6. Huynh, C., et al. Defective lysosomal exocytosis and plasma membrane repair in Chediak-Higashi/beige cells. *Proceeding of the National Academy of Sciences of the United States of America.* **101** (48), 16795-800 (2004).
7. Cooper, S.T., McNeil, P.L. Membrane Repair: Mechanisms and Pathophysiology. *Physiological Reviews*. **95** (4), 1205-40 (2015).
8. Steinhardt, R.A., Bi G., J.M. Alderton J.M. *C*ell membrane resealing by a vesicular mechanism similar to neurotransmitter release. *Science.* **263** (5145), 390-3 (1994).
9. De Mello, W.C. Membrane sealing in frog skeletal-muscle fibers. *Proceedings of the National Academy of Sciences of the United States of America*. **70** (4), 982-4 (1973).
10. Fishman, H.M., Tewari K.P., Stein P.G. Injury-induced vesiculation and membrane redistribution in squid giant axon. *Biochimica et Biophysica Acta.* **1023** (3), 421-35 (1990).

11. Davenport, N.R., Bement, W.M. Cell repair: Revisiting the patch hypothesis. *Communicative & Integrative Biology*. **9** (6), e1253643 (2016).
12. McNeil, P.L., et al. Patching plasma membrane disruptions with cytoplasmic membrane. *Journal of Cell Science.* **113** (11), 1891-902 (2000).
13. Terasaki, M., Miyake, K., McNeil, P.L. Large plasma membrane disruptions are rapidly resealed by Ca2+-dependent vesicle-vesicle fusion events. *Journal of Cell Biology.* **139** (1), 63-74 (1997).
14. Bi, G.Q., Alderton, J.M., Steinhardt, R.A. Calcium-regulated exocytosis is required for cell membrane resealing. *Journal of Cell Biology.* **131** (6 Pt. 2), 1747-58 (1995).
15. Tam, C., et al. Exocytosis of acid sphingomyelinase by wounded cells promotes endocytosis and plasma membrane repair. *Journal of Cell Biology.* **189** (6), 1027-38 (2010).
16. Rodriguez, A., et al. Lysosomes behave as Ca2+-regulated exocytic vesicles in fibroblasts and epithelial cells. *Journal of Cell Biology.* **137** (1), 93-104 (1997).
17. Reddy, A., Caler, E.V., Andrews, N.W. Plasma membrane repair is mediated by Ca(2+)-regulated exocytosis of lysosomes. *Cell*. **106** (2), 157-69 (2001).
18. Jimenez, A.J., et al. ESCRT machinery is required for plasma membrane repair. *Science*. **343** (6174), 1247136 (2014).
19. Pathak-Sharma, S., et al. High-Throughput Microplate-Based Assay to Monitor Plasma Membrane Wounding and Repair. *Frontiers in Cellular and Infection Microbiology*. **7**, 305 (2017).
20. Hamon, M.A., et al. Listeriolysin O: the Swiss army knife of Listeria. *Trends in Microbiology.* **20** (8), 360-8 (2012).
21. Seveau, S., Multifaceted activity of listeriolysin O, the cholesterol-dependent cytolysin of Listeria monocytogenes. *Subcellular Biochemistry.* **80**, 161-95 (2014).
22. Osborne, S.E., Brumell, J.H. Listeriolysin O: from bazooka to Swiss army knife. *Philosophical Transactions of the Royal Society of London B: Biological Sciences.* **372** (1726), (2017).
23. Lukoyanova, N., Hoogenboom, B.W., Saibil, H.R. The membrane attack complex, perforin and cholesterol-dependent cytolysin superfamily of pore-forming proteins. *Journal of Cell Science.* **129** (11), 2125-33 (2016).
24. Tweten, R.K. Cholesterol-dependent cytolysins, a family of versatile pore-forming toxins. *Infection and Immunity.* **73** (10), 6199-209 (2005).
25. Koster, S., et al. Crystal structure of listeriolysin O reveals molecular details of oligomerization and pore formation. *Nature Communications.* **5**, 3690 (2014).
26. Duncan, J.L., Schlegel, R. Effect of streptolysin O on erythrocyte membranes, liposomes, and lipid dispersions. A protein-cholesterol interaction. *Journal of Cell Biology.* **67** (1), 160-74 (1975).
27. Morgan, P.J., et al. Subunit organisation and symmetry of pore-forming, oligomeric pneumolysin. *FEBS Letters.* **371** (1), 77-80 (1995).
28. Leung, C., et al. Stepwise visualization of membrane pore formation by suilysin, a bacterial cholesterol-dependent cytolysin. *eLife.* **3**, e04247 (2014).
29. Marchioretto, M., et al. What planar lipid membranes tell us about the pore-forming activity of cholesterol-dependent cytolysins. *Biophysical Chemistry.* **182**, 64-70 (2013).
30. Palmer, M., et al. Assembly mechanism of the oligomeric streptolysin O pore: the early membrane lesion is lined by a free edge of the lipid membrane and is extended gradually during

oligomerization. *European Molecular Biology Organization Journal.* **17** (6), 1598-605 (1998).
31. Bavdek, A., et al. pH dependence of listeriolysin O aggregation and pore-forming ability. *Federation of European Biochemical Society Journal.* **279** (1), 126-41 (2012).
32. Schuerch, D.W., Wilson-Kubalek, E.M., Tweten, R.K. Molecular basis of listeriolysin O pH dependence. *Proceeding of the National Academy of Sciences of the United States of America*. **102** (35), 12537-42 (2005).
33. Cassidy, S.K., O'Riordan, M.X. *M*ore than a pore: the cellular response to cholesterol-dependent cytolysins. *Toxins (Basel*). **5** (4), 618-36 (2013).
34. Lam, J., et al. Host cell perforation by listeriolysin O (LLO) activates a Ca(2+)-dependent cPKC/Rac1/Arp2/3 signaling pathway that promotes L. monocytogenes internalization independently of membrane resealing. *Molecular Biology of the Cell.* (2017).
35. Gekara, N.O., Weiss, S. Lipid rafts clustering and signalling by listeriolysin O. *Biochemical Society Transactions.* **32** (Pt 5), 712-4 (2004).
36. Magassa, N., Chandrasekaran, S., Caparon, M.G. Streptococcus pyogenes cytolysin-mediated translocation does not require pore formation by streptolysin O. *European Molecular Biology Organization Reports.* **11** (5), 400-5 (2010).
37. Baba, H., et al. Induction of gamma interferon and nitric oxide by truncated pneumolysin that lacks pore-forming activity. *Infection and Immunity.* **70** (1), 107-13 (2002).
38. Carrero, J.A., Vivanco-Cid, H., Unanue, E.R. Listeriolysin o is strongly immunogenic independently of its cytotoxic activity. *Public Library of Science One*. **7** (3), e32310 (2012).
39. Coconnier, M.H., et al. Listeriolysin O-induced stimulation of mucin exocytosis in polarized intestinal mucin-secreting cells: evidence for toxin recognition of membrane-associated lipids and subsequent toxin internalization through caveolae. *Cell Microbiology.* **2** (6), 487-504 (2000).
40. Suzuki, T., et al. DNA staining for fluorescence and laser confocal microscopy. *Journal of Histochemistry and Cytochemistry.* **45** (1), 49-53 (1997).
41. Bink, K., et al. TO-PRO-3 is an optimal fluorescent dye for nuclear counterstaining in dual-colour FISH on paraffin sections. *Histochemistry and Cell Biology.* **115** (4), 293-9 (2001).
42. Zhang, J.H., Chung, T.D., Oldenburg, K.R. A Simple Statistical Parameter for Use in Evaluation and Validation of High Throughput Screening Assays. *Journal of Biomolecular Screening.* **4** (2), 67-73 (1999).
43. Birmingham, A., et al. Statistical methods for analysis of high-throughput RNA interference screens. *Nature Methods.* **6** (8), 569-75 (2009).
44. Zhang, X.D. A pair of new statistical parameters for quality control in RNA interference high-throughput screening assays. *Genomics.* **89** (4), 552-61 (2007).
45. Zhang, X.D. A new method with flexible and balanced control of false negatives and false positives for hit selection in RNA interference high-throughput screening assays. *Journal of Biomolecular Screening*. **12** (5), 645-55 (2007).
46. Idone, V., et al. Repair of injured plasma membrane by rapid Ca2+-dependent endocytosis. *Journal of Cell Biology.* **180** (5), 905-14 (2008).
47. Davenport, N.R., et al. Membrane dynamics during cellular wound repair. *Molecular Biology of the Cell.* **27** (14), 2272-85 (2016).
48. Defour, A., Sreetama, S.C., Jaiswal, J.K. Imaging cell membrane injury and subcellular processes involved in repair. *Journal of Visualized Experiments*. **85**, (2014).
49. Lee, J.J.A., et al. Cell Membrane Repair Assay Using a Two-photon Laser Microscope.

Journal of Visualized Experiments. (131), 2018.
50. Weisleder, N., et al. Visualization of MG53-mediated cell membrane repair using in vivo and in vitro systems. *Journal of Visualized Experiments.* (52), (2011).
51. Corrotte, M., et al. Toxin pores endocytosed during plasma membrane repair traffic into the lumen of MVBs for degradation. *Traffic.* **13** (3), 483-94 (2012).
52. Kuismanen, E., Saraste, J. Low temperature-induced transport blocks as tools to manipulate membrane traffic*. Methods in Cell Biology*. **32**, 257-74 (1989).
53. Togo, T., et al. The mechanism of facilitated cell membrane resealing. *Journal of Cell Science.* **112** (Pt 5), 719-31 (1999).
54. Johnson, S.A., et al. Temperature-dependent phase behavior and protein partitioning in giant plasma membrane vesicles. *Biochimica et Biophysica Acta.* **1798** (7), 1427-35 (2010).
55. Lam, J.G.T., et al. Host cell perforation by listeriolysin O (LLO) activates a Ca(2+)-dependent cPKC/Rac1/Arp2/3 signaling pathway that promotes Listeria monocytogenes internalization independently of membrane resealing. *Molecular Biology of the Cell.* **29** (3), 270-284 (2018).

Figure1

Click here to download Figure Slide1.TIF

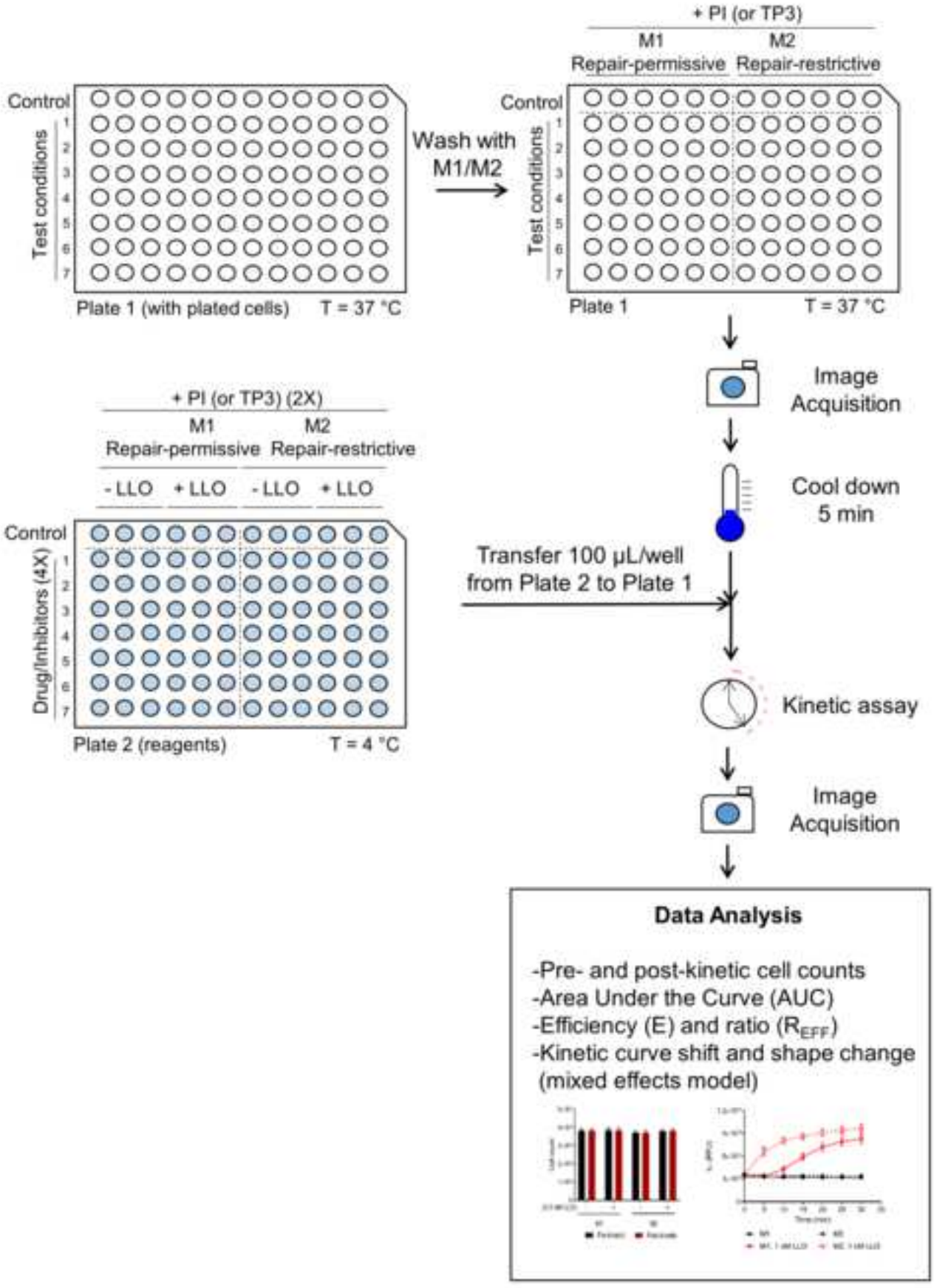

Figure2

Click here to download Figure Slide2.TIF

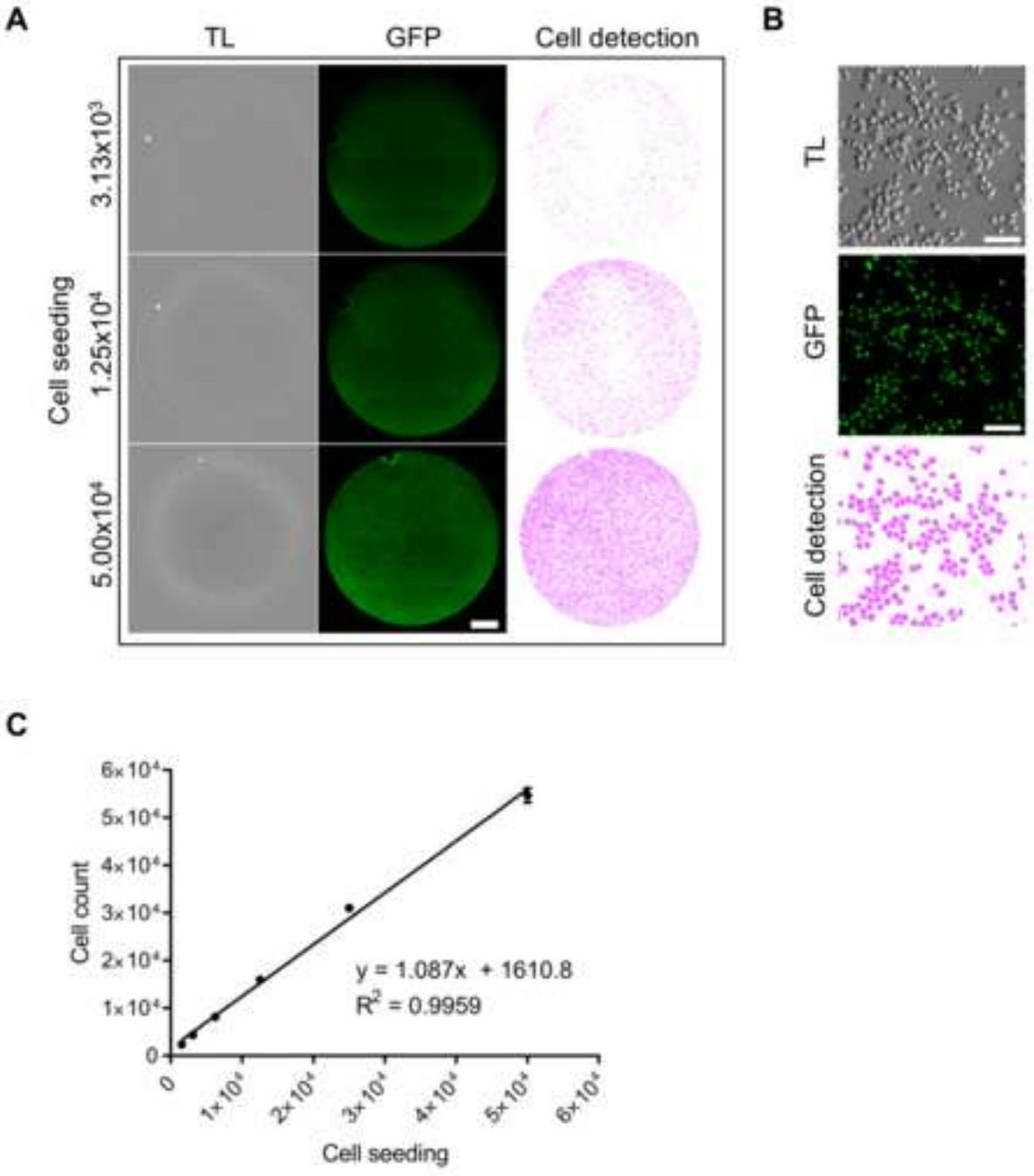

Figure3

Click here to download Figure Slide3.TIF

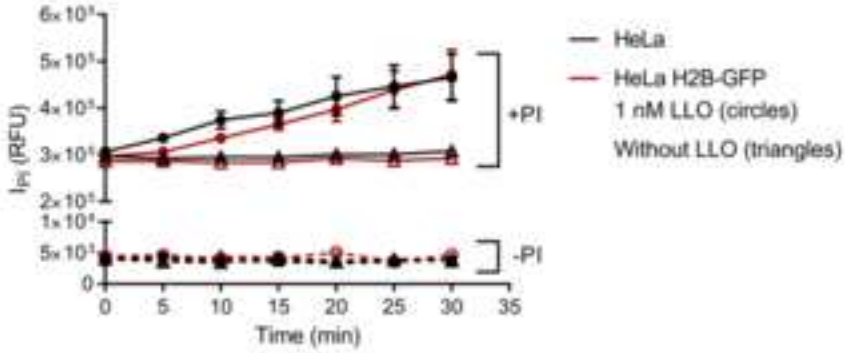

Figure4

Click here to download Figure Slide4.TIF

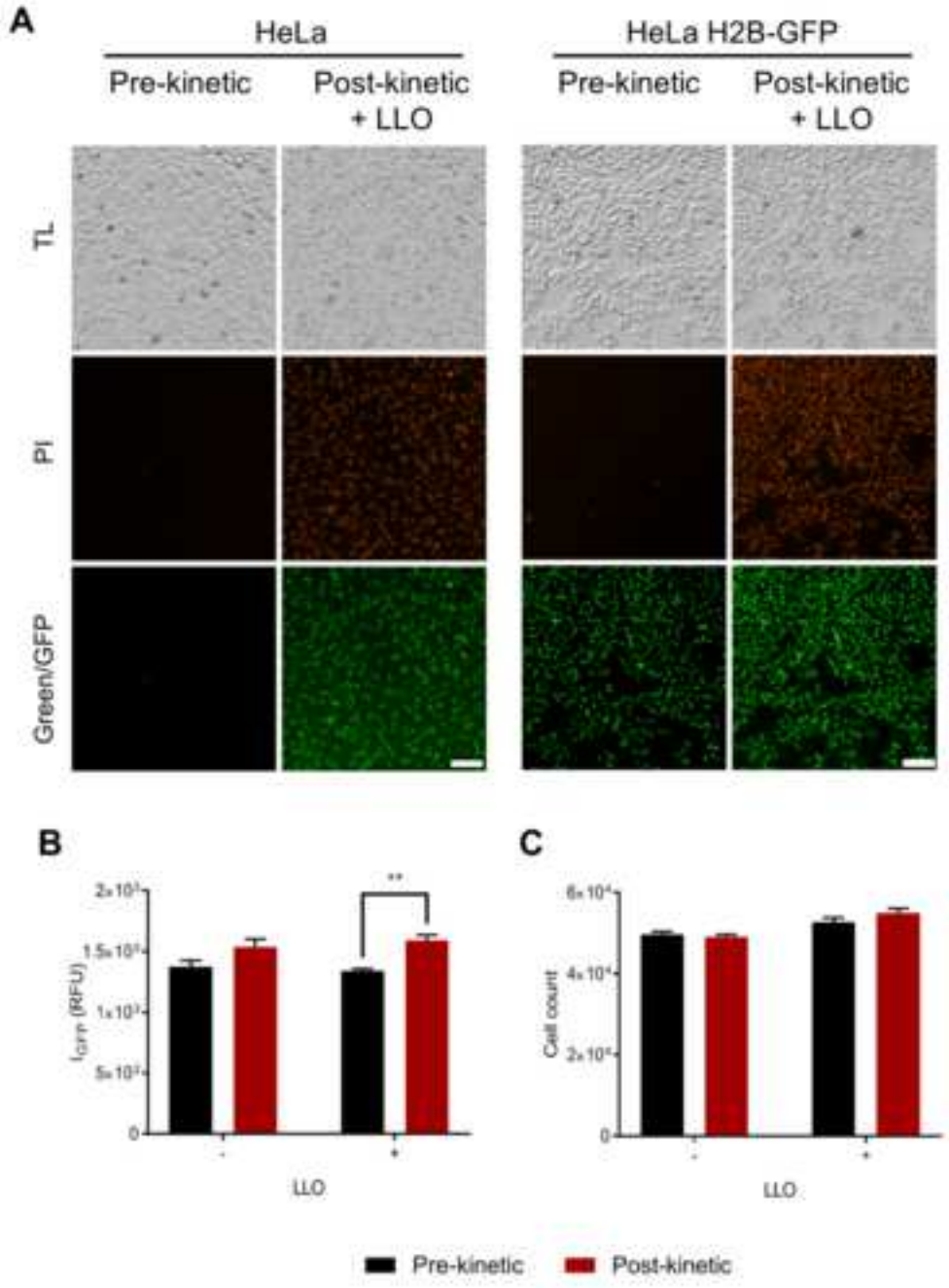

Figure5

Click here to download Figure Slide5.TIF

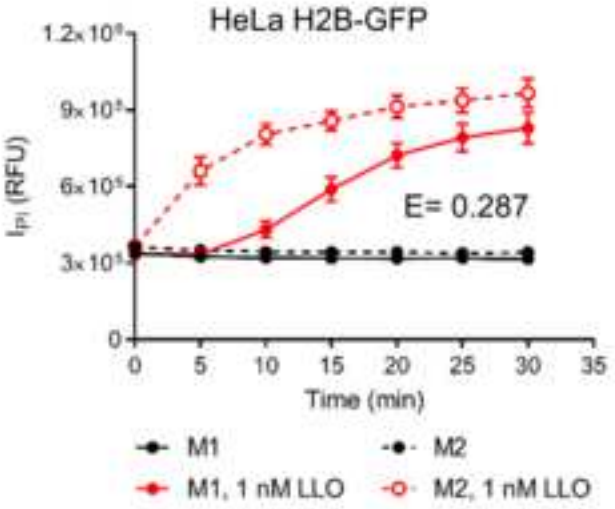

Figure6

Click here to download Figure Slide6.TIF

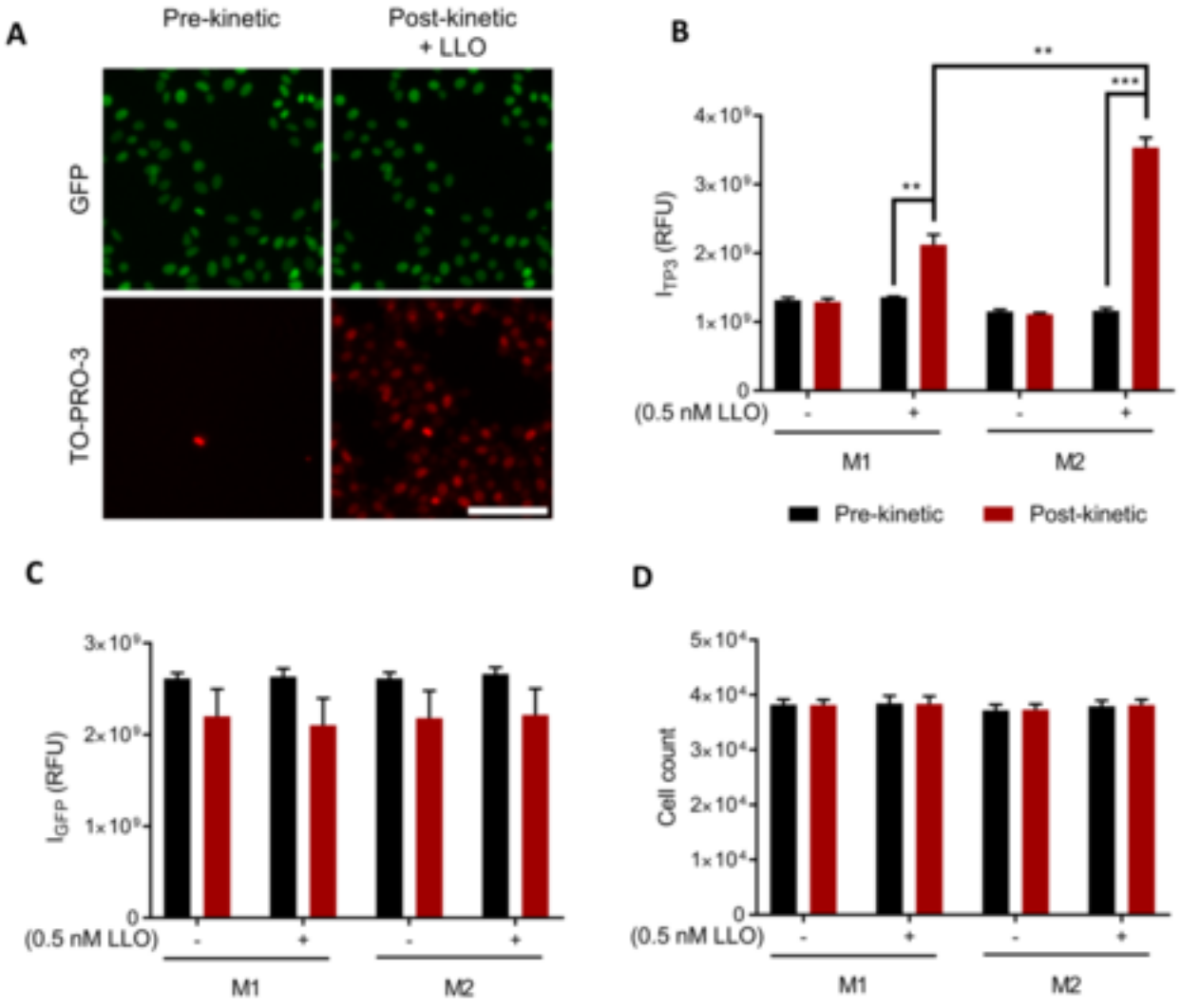

Figure7

Click here to download Figure Slide7.TIF

A

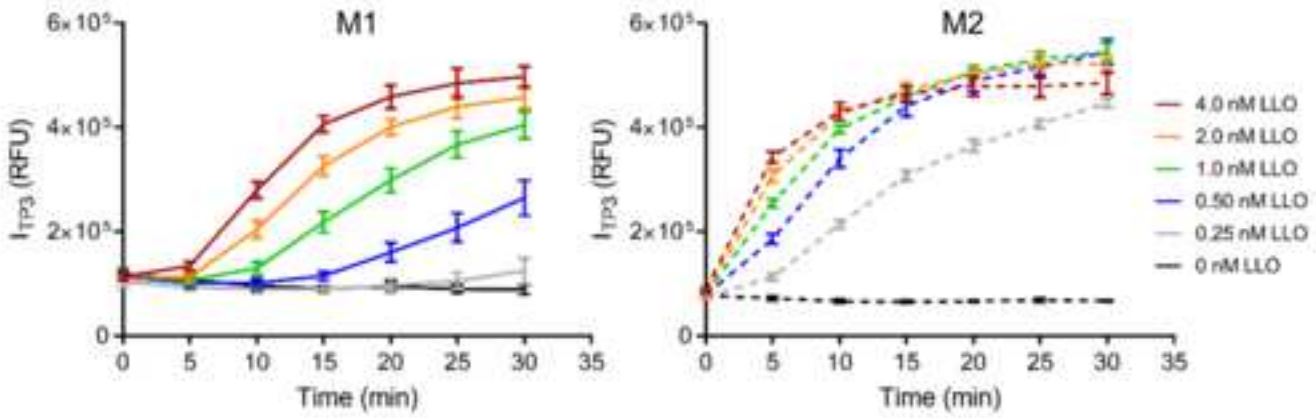

B

LLO (nM)	AUC(M1)	AUC(M2)	Z-factor	SSMD (β)	E
0.25	2966852	8323250	0.372	6.715	**0.643546**
0.50	4395097	1140392	0.064	4.494	**0.614647**
1.00	6912908	12293067	-0.491	2.780	**0.437658**
2.00	8837675	12647264	-1.953	1.431	**0.301218**
4.00	10329587	12400673	-21.721	0.186	**0.167014**

Figure8 Click here to download Figure Slide8.TIF

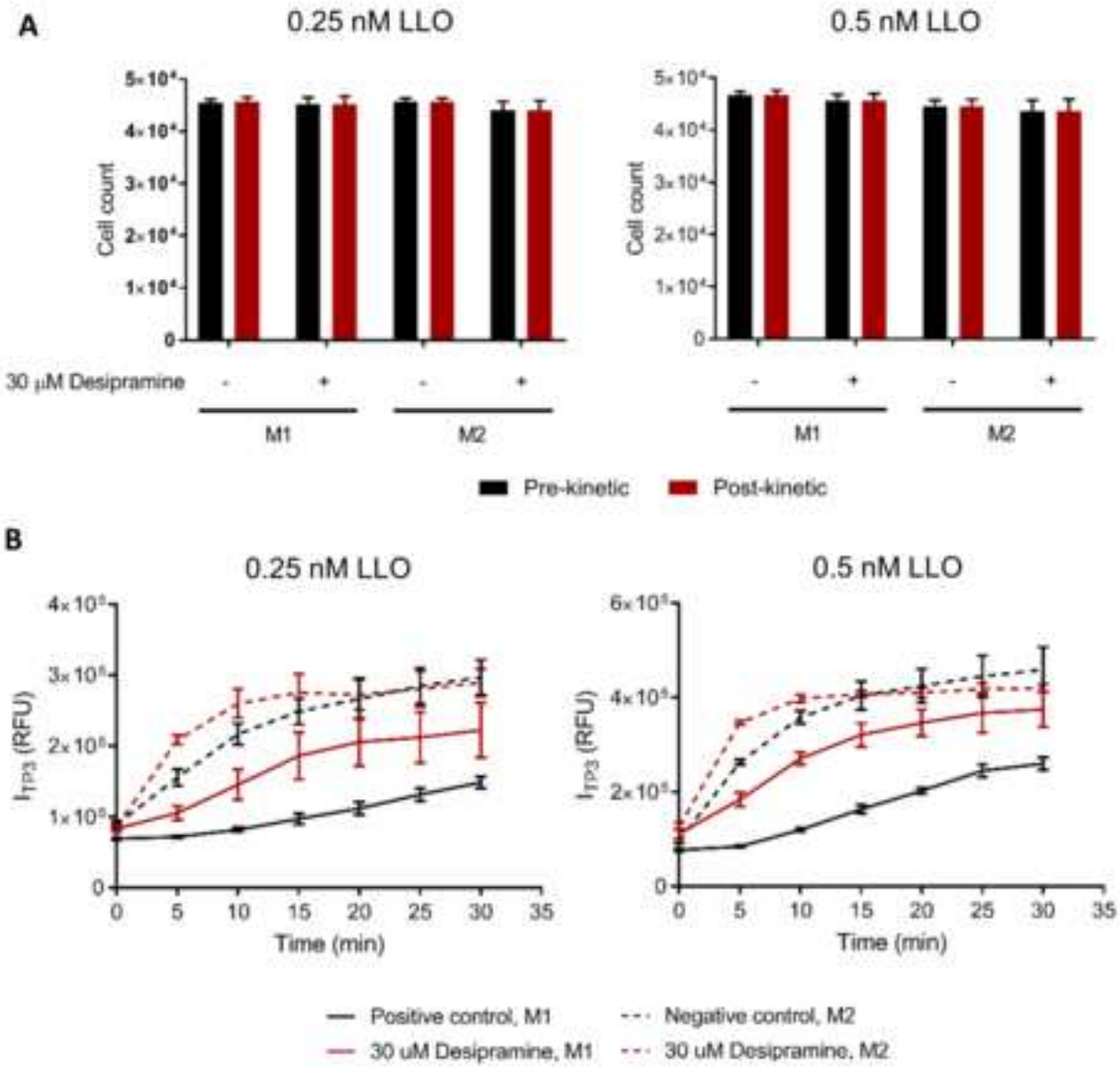

C

	0.25 nM LLO	0.5 nM LLO
$E_{Control}$	0.5575	0.5266
$E_{Desipramine}$	0.3206	0.2433
R_{Eff}	**0.5752**	**0.4621**
p-value **(mixed effect model)**	**0.0010**	**$1x10^{-10}$**

Table 1

		Imaging Cytometer Emission Channel Specifications	
Fluorophore	Fluorophore ex/em (nm)	Green channel (ex/em ± bandpass, nm)	Red channel (ex/em ± bandpass, nm)
GFP	488/510	460/541 ± 20/108	625/713 ± 20/123
PI	533/617		
CNABD	642/661		

Materials Table

Click here to download Table of Materials Materials.xls

Name of Material/ Equipment	Company	Catalog Number	Comments/Description
SpectraMax i3x Multi-Mode Microplate Reader	Molecular Devices	i3x	
MiniMax 300 Imaging cytometer	Molecular Devices	5024062	
TO-PRO-3	ThermoFisher Scientific	T3605	
Propidium Iodide	ThermoFisher Scientific	P3566	
HeLa	ATCC	CCL2	
HeLa H2B-GFP	Millipore	SCC117	
Trypsin-EDTA 0.25%	ThermoFisher Scientific	25200056	
96-well Corning flat bottom black polystyrene tissue culture treated plate	Corning	3603	
Hanks' balanced Salts	Sigma-Aldrich	H4891	
EGTA	ISC BioExpress	0732-100G	
HEPES	Fisher Scientific	BP310-500	
D-(+)-Glucose, HybriMax	Sigma-Aldrich	G5146-1KG	

jove JOURNAL OF VISUALIZED EXPERIMENTS
1 Alewife Center #200
Cambridge, MA 02140
tel. 617.945.9051
www.jove.com

ARTICLE AND VIDEO LICENSE AGREEMENT

Title of Article: Kinetic measurement of plasma membrane resealing efficiency in fluorescent cells using a high-throughput assay

Author(s): Jonathan G.T. Lam and Stephanie Seveau

Item 1 (check one box): The Author elects to have the Materials be made available (as described at http://www.jove.com/author) via: ☑ Standard Access ☐ Open Access

Item 2 (check one box):

☑ The Author is NOT a United States government employee.

☐ The Author is a United States government employee and the Materials were prepared in the course of his or her duties as a United States government employee.

☐ The Author is a United States government employee but the Materials were NOT prepared in the course of his or her duties as a United States government employee.

ARTICLE AND VIDEO LICENSE AGREEMENT

1. Defined Terms. As used in this Article and Video License Agreement, the following terms shall have the following meanings: "**Agreement**" means this Article and Video License Agreement; "**Article**" means the article specified on the last page of this Agreement, including any associated materials such as texts, figures, tables, artwork, abstracts, or summaries contained therein; "**Author**" means the author who is a signatory to this Agreement; "**Collective Work**" means a work, such as a periodical issue, anthology or encyclopedia, in which the Materials in their entirety in unmodified form, along with a number of other contributions, constituting separate and independent works in themselves, are assembled into a collective whole; "**CRC License**" means the Creative Commons Attribution-Non Commercial-No Derivs 3.0 Unported Agreement, the terms and conditions of which can be found at: http://creativecommons.org/licenses/by-nc-nd/3.0/legalcode; "**Derivative Work**" means a work based upon the Materials or upon the Materials and other pre-existing works, such as a translation, musical arrangement, dramatization, fictionalization, motion picture version, sound recording, art reproduction, abridgment, condensation, or any other form in which the Materials may be recast, transformed, or adapted; "**Institution**" means the institution, listed on the last page of this Agreement, by which the Author was employed at the time of the creation of the Materials; "**JoVE**" means MyJove Corporation, a Massachusetts corporation and the publisher of *The Journal of Visualized Experiments*; "**Materials**" means the Article and / or the Video; "**Parties**" means the Author and JoVE; "**Video**" means any video(s) made by the Author, alone or in conjunction with any other parties, or by JoVE or its affiliates or agents, individually or in collaboration with the Author or any other parties, incorporating all or any portion of the Article, and in which the Author may or may not appear.

2. Background. The Author, who is the author of the Article, in order to ensure the dissemination and protection of the Article, desires to have the JoVE publish the Article and create and transmit videos based on the Article. In furtherance of such goals, the Parties desire to memorialize in this Agreement the respective rights of each Party in and to the Article and the Video.

3. Grant of Rights in Article. In consideration of JoVE agreeing to publish the Article, the Author hereby grants to JoVE, subject to **Sections 4** and **7** below, the exclusive, royalty-free, perpetual (for the full term of copyright in the Article, including any extensions thereto) license (a) to publish, reproduce, distribute, display and store the Article in all forms, formats and media whether now known or hereafter developed (including without limitation in print, digital and electronic form) throughout the world, (b) to translate the Article into other languages, create adaptations, summaries or extracts of the Article or other Derivative Works (including, without limitation, the Video) or Collective Works based on all or any portion of the Article and exercise all of the rights set forth in (a) above in such translations, adaptations, summaries, extracts, Derivative Works or Collective Works and (c) to license others to do any or all of the above. The foregoing rights may be exercised in all media and formats, whether now known or hereafter devised, and include the right to make such modifications as are technically necessary to exercise the rights in other media and formats. If the "Open Access" box has been checked in **Item 1** above, JoVE and the Author hereby grant to the public all such rights in the Article as provided in, but subject to all limitations and requirements set forth in, the CRC License.

4. Retention of Rights in Article. Notwithstanding the exclusive license granted to JoVE in **Section 3** above, the Author shall, with respect to the Article, retain the non-exclusive right to use all or part of the Article for the non-commercial purpose of giving lectures, presentations or teaching classes, and to post a copy of the Article on the Institution's website or the Author's personal website, in each case provided that a link to the Article on the JoVE website is provided and notice of JoVE's copyright in the Article is included. All non-copyright intellectual property rights in and to the Article, such as patent rights, shall remain with the Author.

5. Grant of Rights in Video – Standard Access. This **Section 5** applies if the "Standard Access" box has been checked in **Item 1** above or if no box has been checked in **Item 1** above. In consideration of JoVE agreeing to produce, display or otherwise assist with the Video, the Author hereby acknowledges and agrees that, Subject to **Section 7** below, JoVE is and shall be the sole and exclusive owner of all rights of any nature, including, without limitation, all copyrights, in and to the Video. To the extent that, by law, the Author is deemed, now or at any time in the future, to have any rights of any nature in or to the Video, the Author hereby disclaims all such rights and transfers all such rights to JoVE.

6. Grant of Rights in Video – Open Access. This **Section 6** applies only if the "Open Access" box has been checked in **Item 1** above. In consideration of JoVE agreeing to produce, display or otherwise assist with the Video, the Author hereby grants to JoVE, subject to **Section 7** below, the exclusive, royalty-free, perpetual (for the full term of copyright in the Article, including any extensions thereto) license (a) to publish, reproduce, distribute, display and store the Video in all forms, formats and media whether now known or hereafter developed (including without limitation in print, digital and electronic form) throughout the world, (b) to translate the Video into other languages, create adaptations, summaries or extracts of the Video or other Derivative Works or Collective Works based on all or any portion of the Video and exercise all of the rights set forth in (a) above in such translations, adaptations, summaries, extracts, Derivative Works or Collective Works and (c) to license others to do any or all of the above. The foregoing rights may be exercised in all media and formats, whether now known or hereafter devised, and include the right to make such modifications as are technically necessary to exercise the rights in other media and formats. For any Video to which this Section 6 is applicable, JoVE and the Author hereby grant to the public all such rights in the Video as provided in, but subject to all limitations and requirements set forth in, the CRC License.

7. Government Employees. If the Author is a United States government employee and the Article was prepared in the course of his or her duties as a United States government employee, as indicated in **Item 2** above, and any of the licenses or grants granted by the Author hereunder exceed the scope of the 17 U.S.C. 403, then the rights granted hereunder shall be limited to the maximum rights permitted under such statute. In such case, all provisions contained herein that are not in conflict with such statute shall remain in full force and effect, and all provisions contained herein that do so conflict shall be deemed to be amended so as to provide to JoVE the maximum rights permissible within such statute.

8. Likeness, Privacy, Personality. The Author hereby grants JoVE the right to use the Author's name, voice, likeness, picture, photograph, image, biography and performance in any way, commercial or otherwise, in connection with the Materials and the sale, promotion and distribution thereof. The Author hereby waives any and all rights he or she may have, relating to his or her appearance in the Video or otherwise relating to the Materials, under all applicable privacy, likeness, personality or similar laws.

9. Author Warranties. The Author represents and warrants that the Article is original, that it has not been published, that the copyright interest is owned by the Author (or, if more than one author is listed at the beginning of this Agreement, by such authors collectively) and has not been assigned, licensed, or otherwise transferred to any other party. The Author represents and warrants that the author(s) listed at the top of this Agreement are the only authors of the Materials. If more than one author is listed at the top of this Agreement and if any such author has not entered into a separate Article and Video License Agreement with JoVE relating to the Materials, the Author represents and warrants that the Author has been authorized by each of the other such authors to execute this Agreement on his or her behalf and to bind him or her with respect to the terms of this Agreement as if each of them had been a party hereto as an Author. The Author warrants that the use, reproduction, distribution, public or private performance or display, and/or modification of all or any portion of the Materials does not and will not violate, infringe and/or misappropriate the patent, trademark, intellectual property or other rights of any third party. The Author represents and warrants that it has and will continue to comply with all government, institutional and other regulations, including, without limitation all institutional, laboratory, hospital, ethical, human and animal treatment, privacy, and all other rules, regulations, laws, procedures or guidelines, applicable to the Materials, and that all research involving human and animal subjects has been approved by the Author's relevant institutional review board.

10. JoVE Discretion. If the Author requests the assistance of JoVE in producing the Video in the Author's facility, the Author shall ensure that the presence of JoVE employees, agents or independent contractors is in accordance with the relevant regulations of the Author's institution. If more than one author is listed at the beginning of this Agreement, JoVE may, in its sole discretion, elect not take any action with respect to the Article until such time as it has received complete, executed Article and Video License Agreements from each such author. JoVE reserves the right, in its absolute and sole discretion and without giving any reason therefore, to accept or decline any work submitted to JoVE. JoVE and its employees, agents and independent contractors shall have

jove JOURNAL OF VISUALIZED EXPERIMENTS
1 Alewife Center #200
Cambridge, MA 02140
tel. 617.945.9051
www.jove.com

ARTICLE AND VIDEO LICENSE AGREEMENT

full, unfettered access to the facilities of the Author or of the Author's institution as necessary to make the Video, whether actually published or not. JoVE has sole discretion as to the method of making and publishing the Materials, including, without limitation, to all decisions regarding editing, lighting, filming, timing of publication, if any, length, quality, content and the like.

11. Indemnification. The Author agrees to indemnify JoVE and/or its successors and assigns from and against any and all claims, costs, and expenses, including attorney's fees, arising out of any breach of any warranty or other representations contained herein. The Author further agrees to indemnify and hold harmless JoVE from and against any and all claims, costs, and expenses, including attorney's fees, resulting from the breach by the Author of any representation or warranty contained herein or from allegations or instances of violation of intellectual property rights, damage to the Author's or the Author's institution's facilities, fraud, libel, defamation, research, equipment, experiments, property damage, personal injury, violations of institutional, laboratory, hospital, ethical, human and animal treatment, privacy or other rules, regulations, laws, procedures or guidelines, liabilities and other losses or damages related in any way to the submission of work to JoVE, making of videos by JoVE, or publication in *JoVE* or elsewhere by JoVE. The Author shall be responsible for, and shall hold JoVE harmless from, damages caused by lack of sterilization, lack of cleanliness or by contamination due to the making of a video by JoVE its employees, agents or independent contractors. All sterilization, cleanliness or decontamination procedures shall be solely the responsibility of the Author and shall be undertaken at the Author's expense. All indemnifications provided herein shall include JoVE's attorney's fees and costs related to said losses or damages. Such indemnification and holding harmless shall include such losses or damages incurred by, or in connection with, acts or omissions of JoVE, its employees, agents or independent contractors.

12. Fees. To cover the cost incurred for publication, JoVE must receive payment before production and publication the Materials. Payment is due in 21 days of invoice. Should the Materials not be published due to an editorial or production decision, these funds will be returned to the Author. Withdrawal by the Author of any submitted Materials after final peer review approval will result in a US$1,200 fee to cover pre-production expenses incurred by JoVE. If payment is not received by the completion of filming, production and publication of the Materials will be suspended until payment is received.

13. Transfer, Governing Law. This Agreement may be assigned by JoVE and shall inure to the benefits of any of JoVE's successors and assignees. This Agreement shall be governed and construed by the internal laws of the Commonwealth of Massachusetts without giving effect to any conflict of law provision thereunder. This Agreement may be executed in counterparts, each of which shall be deemed an original, but all of which together shall be deemed to me one and the same agreement. A signed copy of this Agreement delivered by facsimile, e-mail or other means of electronic transmission shall be deemed to have the same legal effect as delivery of an original signed copy of this Agreement.

A signed copy of this document must be sent with all new submissions. Only one Agreement required per submission.

CORRESPONDING AUTHOR:

Name: Stephanie Seveau

Department: Microbial Infection and Immunity

Institution: The Ohio State University

Article Title: Kinetic measurement of plasma membrane resealing efficiency in fluorescent cells using a high-throughput assay

Signature: Seveau SS Date: 4-24-18

Please submit a signed and dated copy of this license by one of the following three methods:

1) Upload a scanned copy of the document as a pfd on the JoVE submission site;
2) Fax the document to +1.866.381.2236;
3) Mail the document to JoVE / Attn: JoVE Editorial / 1 Alewife Center #200 / Cambridge, MA 02139

For questions, please email submissions@jove.com or call +1.617.945.9051

THE OHIO STATE UNIVERSITY
COLLEGE OF MEDICINE

Microbial Infection and Immunity
Stephanie M Seveau, Associate Professor

786 Biomedical Research Tower
460 W. 12th Avenue
Columbus, OH 43210-2210
Phone: 614-247-7671
Fax: 614-292-9616

July 3rd, 2018

Dear Editor,

I have the pleasure to submit the revised version of the method manuscript entitled: "High-Throughput Measurement of the Plasma Membrane Resealing Efficiency in Mammalian Cells". We are thankful to the reviewers and editorial team for their very insightful comments. Based upon these comments, we have thoroughly re-written the entire manuscript to increase its clarity. We also shortened and clarified the abstract, which was providing too many complicated details. The title was modified to remove the word "kinetic", as this term was misleading. Indeed, one reviewer thought that our goal was to measure the kinetic of plasma membrane resealing, but this is not the case. We use a kinetic assay that assesses the cell resealing efficiency over time, but does not measure how long it takes a given cell to reseal a given toxin pore. We also removed Table 1, as this table was providing unnecessary redundant information. We re-evaluated the analytical methods of this manuscript with the precious help of Dr. Chi Song from the Division of Biostatistics (OSU). We included calculation of the resealing efficiency, which characterizes the ability of cells to undergo plasma membrane resealing in any given experimental condition. We also calculated Z-factor and SSMD, and included intra-experiment statistical tools. Additional experiments were performed, as for example providing proof of concept, as requested by a reviewer. Below is a point-by-point answer to all comments we received.

Stephanie Seveau, PhD

Editorial comments:

-Figure 1: Please include a space between number and its corresponding unit (e.g., 37 °C, 4 °C). Please also change "µl" to "µL".
We performed these changes.

-Figure 2: Please make the scale bar line thicker/darker in panel A so it is easier to read.
A larger scale bar was made in Figure 2A matching the thickness of the scale bars in Figure 2B.

-Please provide an email address for each author.
An email address was provided for each author. **Lines 16, 17, 20.**

-Please use SI abbreviations for all units: L, mL, µL, h, min, s, etc.
We performed these changes.

-Please include a space between all numbers and their corresponding units: 15 mL, 37 °C, 60 s; etc.
This was corrected.

-Please revise the protocol text to avoid the use of any personal pronouns (e.g., "we", "you", "our" etc.).
This was corrected.

-JoVE cannot publish manuscripts containing commercial language. This includes trademark symbols (™), registered symbols (®), and company names before an instrument or reagent. Please remove all commercial language from your manuscript and use generic terms instead. All commercial products should be sufficiently referenced in the Table of Materials and Reagents. For example: ATCC®, EMD Millipore, Corning, SpectraMax, Axygen Scientific, SoftMax Pro7, etc.
All commercial language was removed

-Please revise the protocol to contain only action items that direct the reader to do something. The actions should be described in the imperative tense in complete sentences wherever possible. Avoid usage of phrases such as "could be," "should be," and "would be" throughout the Protocol. Any text that cannot be written in the imperative tense may be added as a "Note."
This was corrected.

1.1.1: Please specify cell type, cell culture medium, and the volume of Trypsin-EDTA 0.25% used.
This was corrected. **Lines 136-140.**

1.1.2: Please provide the composition of growth medium used.
The composition of growth medium was specified. **Lines 145-146.**

-Please include single-line spaces between all paragraphs, headings, steps, etc.
Single line spaces were placed between all paragraphs and steps.

-Please revise to explain the Representative Results in the context of the technique you have described, e.g., how do these results show the technique, suggestions about how to analyze the outcome, etc. The paragraph text should refer to all of the figures. Data from both

successful and sub-optimal experiments can be included.
This was accordingly corrected.

-References: Please do not abbreviate journal titles.
All journal titles are written in full. **Lines 706-835.**

Reviewers' comments:

Reviewer #1:
1. Although the appropriate controls are outlined, there is a lack of statistical test to determine if this assay is robust enough for a high-throughput screen. Can the authors perform a statistical test such as the Z-factor (Z') (or other commonly used test) to assess a good discrimination between negative and positive controls?
Birmingham, Amanda; et al. (August 2009). "Statistical Methods for Analysis of High-Throughput RNA Interference Screens". Nat Methods. 6 (8): 569-575. doi:10.1038/nmeth.1351
We established a collaboration with Dr. Chi Song from the Division of Biostatistics (OSU) to re-evaluate the analytical methods. Z-factor and SSMD (strictly standardized mean difference) were determined to assess the robustness of the membrane repair assay. We also introduced a mixed effect model to provide statistical power within a single high-throughput screen involving four technical replicates. **Figure 7, lines 471-498, 594-602, 682-689**

2. As a proof-of-principle, can the authors show a defect in membrane repair using an siRNA or drug target known to be involved in plasma membrane resealing (e.g. Annexins, ESCRT, etc.)?
HeLa H2B-GFP cells were treated with the chemical inhibitor desipramine, which was previously shown to block membrane repair presumably via inhibition of the acid sphingomyelinase (ASM). Data presented in Figure 8 and corresponding analyses confirm that this drug inhibits membrane resealing, as evidenced by a decrease in the resealing efficiency measured in the presence of the drug. **Lines 500-522, Figure 8, and 604-617.**

3. This method article is based on a previously published method article, which should be cited.
Pathak-Sharma, S., Zhang, X., Lam, J. G. T., Weisleder, N., & Seveau, S. M. (2017). High-Throughput Microplate-Based Assay to Monitor Plasma Membrane Wounding and Repair. Frontiers in Cellular and Infection Microbiology, 7, 305. http://doi.org/10.3389/fcimb.2017.00305
Pathak Sharma et al. was referenced in the introduction. **Lines 80 and 137.**

4. Figure 3 is similar to Figure 4A/B and therefore can be remove.
Figures have been remodeled to avoid redundancies, as advised.

5. Line 296 (Results Figure 6), the authors say: "Indeed, HeLa H2B-GFP cells exposed to 0.5 nM LLO in M1 containing 1 μM TO-PRO-3 exhibit a 2-3-fold increase in fluorescence

relative to the non-damaged controls without significantly affecting GFP intensity (Figure 6)." However, Figure 2A shows a 2-fold increase in M1 and a 3-fold increase in M2.
The comment from the reviewer made us realize that the corresponding text lacked clarity. To avoid any confusion, we rephrased this section. **Lines 461-465.**

6. Figure 6E is not described in the results section.
Figure 6E, now figure 7, is described in the results section. It shows the effect of LLO concentration on plasma membrane resealing efficiency. Indeed, efficiency decreases as the concentration of toxin increases. This reflects that high toxin concentrations cause damages that cells cannot repair efficiently. This also shows the LLO concentration range that is best suitable to the assay. **Lines 461-469 and 487-497, Figure 7.**

Reviewer #2:
7. This assay technically is examining cell wounding instead of membrane resealing. As dynamics of dye incorporation showed that intracellular dye concentration kept increasing until saturated.
The assay directly measures cell wounding, as it measures the amount of dye that can penetrate the wounded plasma membrane. This assay also indirectly assesses the efficiency of cell resealing by comparing cell wounding in the presence (M1) and in the absence (M2) of extracellular Ca^{2+} (the latter condition completely prevents repair). To make this point clear, we rephrased the corresponding sections and included an equation for measurement of the resealing efficiency. **Lines 367-384.**

8. I am a little concerned about incubating cells with PI/TO-PRO-3 for 30 min. It is not uncommon for cells to uptake these dyes either through passive transportation or endocytosis.
Some water-soluble dyes can be taken up by pinocytosis. In our experimental conditions, uptake of the dye was negligible. Indeed, controls consisting of cells incubated with PI or TO-PRO-3 (without toxin) showed that there was no detectable increase in fluorescence intensity of the corresponding dyes over the 30 min duration of the kinetic assay **(Figures 3, 5 and 7).**

9. How come cell count is not affected by LLO addition in Fig. 5b? If a cell is wounded and not repaired, GFP would diminish.
HeLa cells do not express a soluble form of GFP; they express the protein chimera Histone 2B-GFP, a nuclear localized protein found in the octameric histone complex, which is wrapped by nuclear DNA and is thus physically immobilized within the nucleus. Despite plasma membrane damage, such nuclear components mostly remain in the nucleus and GFP fluorescence is not lost in damaged cells. In addition, the cell count is not affected by variation in GFP fluorescence intensity as presented in **Figures 4 and 6.**

10. Please describe in the figure legend if cells in Fig. 4C/Fig. 6C is treated with LLO or not.
Treatment conditions were specified in all figure legends.

11. It is recommended to include a Tm-independent positive control for maximal wounding such as cell permeabilizing agent's saponin or triton.
We performed such controls, but they did not bring useful additional information so they were not included.

Reviewer #3:

12. While of higher throughput than many of the mechanical injury approaches in the literature, the toxin used here injures the membrane by extracting cholesterol from the membrane. Due to wide recognition of the role of cholesterol in the membrane signaling and in membrane repair process this limitation of the approach needs to be clearly highlighted in the abstract and elsewhere in the protocol so as to prevent audience from using this approach for membrane injury applications that may be sensitive to cholesterol.
CDC toxins bind to cholesterol, but do not extract cholesterol from the host cell plasma membrane **(lines 85-88).** Due to the high cholesterol content of the plasma membrane and the extremely low active concentration of the toxin, it is unlikely that the toxin affects signaling by affecting cell cholesterol levels. CDCs activate host cell signaling, as we and others have previously published, and this may affect the process of membrane repair as pointed out by the reviewer. This point is now discussed **lines 99-104, 649-653.**

13. As membrane repair is undoubtedly sensitive to physiological temperature, a paragraph dedicated to discussing the limitation of rapid and repeated temperature switching of cells between 4 to 37 degrees on the plasma membrane as well as on the membrane repair process must to be included.
We cannot exclude that temperature switches may affect membrane repair. As suggested, we included a comment relative to temperature switch during the experimental procedure. **Lines 658-661.**

14. The process of membrane repair occurs in seconds to minutes, while the readouts reported here show dye entry that continues for up to half hour, raising questions regarding the relevance of this approach to physiological repair process. As this slow response and readout limits the utility of the approach presented here for studying cellular responses at the seconds time scale that are required for efficient repair, this limitation needs to be discussed.
This assay is not meant to measure the speed of repair in single cells. Its goal is to identify experimental conditions that affect the membrane repair efficiency. We do not need to develop an assay with a milli-sec time resolution to identify a defect in resealing. The previous title may have been misleading as it included the term “kinetic”. The assay is a kinetic assay, but we do not claim measuring the kinetic of repair. This point is now included in the discussion **Lines 542-545.**

15. Previously published protocols in jove (PMID: 29364240, 24686523, 21750489) that avoid some of the above limitations. Discussing these protocols here will benefit the readers and are thus should be included here.

We further explained in the discussion that the previous methods are not high-throughput, which is the goal of the present method. **Lines 636-643.**

16. The table needs cell borders as in its present form it is hard to align the various cells between the different columns.
Table 1: Test conditions was removed.

17. As there are alternate vendors for the microplate reader and imaging cytometer used here, it would be worthwhile to include discussion on if the equipment used here are unique and hence irreplaceable for this protocol or other equipment can also be used.
This type of equipment is offered by different vendors. We learned that Jove policy excludes adding any vendor name, so the specific company's name was removed and we made clear that any plate reader that combines imaging and spectrofluorometry can be used. The described protocol is applicable to any multi-mode plate readers.

Reviewer #4:

18. The protocol in this assay uses PI in the medium during the assay to measure the kinetics of PI influx into the cell. But adding PI at the end of the 30 min repair would also help assess the amount of PI influx that happens by pore formation during the kinetics and the PI influx due to remaining pores (not fully resealed cells). The authors could comment on this variation of the assay to compare PI influxes during pore formation or after repair has failed. Indeed from the kinetics, it is not necessarily clear whether higher doses of LLO cannot be repaired or whether the pores just continue to form over time, allowing PI to enter the cells before the pore is removed from the plasma membrane. Addition of a control condition where PI is added at the end of the repair time frame would address this question.
We agree. We have used such alternative experimental strategy to assess the kinetics of repair of cells damaged by LLO in a distinct research article. The goal of the present approach is to screen for drugs/experimental conditions that affect the repair efficiency, not to measure the kinetic of repair. We removed the term "kinetic" from the title of this manuscript, which was misleading.

19. The authors refer to the kinetics in M1 conditions as reflecting the resealing efficiency, but as such the fluorescence levels recorded reflect the presence of open LLO pores on the plasma membrane and the incorporation of PI into the cells. Therefore, resealing efficiency is better described as the difference between the M2 (repair restrictive where all the formed pores allow for PI entry) and the M1 (repair permissive where some non repaired pores also allow for PI entry) conditions. A change in the text of the abstract and introduction could more specifically address this.
This is correct and we thought that this point was explained in the manuscript. Obviously, we were not sufficiently clear. Therefore, we carefully rephrased the manuscript. We included a method to calculate the resealing efficiency. **Lines 112-116, 367-384, 436-446, 465-469 and Figure 7.**

20. LLO pore formation is not exactly synchronized. The start of pore formation is synchronized when switching to 37 °C, but secondary LLO pores continue to form slowly over time as is illustrated by the progressive increase in PI fluorescence in cells treated with LLO and in the presence of calcium (even at low LLO concentration), a condition where LLO pores should be removed from the plasma membrane and PI stopped from entering further into the cell. If all pores were formed immediately when cells were switched to 37 °c (synchronized), then fluorescence levels would first increase when pores are all formed and then plateau once pores are removed from the plasma membrane. The text should reflect this distinction to explain the progressive increase in PI visible in repair permissible conditions.
We agree, and have clarified this point: only the initiation of pore formation is synchronized. We also better described the formation of pores and the inactivation of the soluble (unbound) form of the toxin. **Lines 93-95, 654-656.**

21. Line 140: This seems to be the first use of the abbreviation PI for propidium iodide and should be indicated here.
The abbreviation for propidium iodide was included **Line 189**

22. Line 150-151: In general, the authors should indicate how the fluorescence reading is organized during the assay (well by well, row by row or the whole plate at once ?). This would help clarify the actual kinetics of the assay when comparing samples in different wells. Can the authors explain how much time the fluorescence reading takes for the whole plate and whether there is a delay between reading the first wells and the last wells of the plate ? Indicating the shortest interval possible between readings would also help readers evaluate the assay's relevance for their own work.
We agree that it is very important information to include. It takes about 30 sec to read the entire 96 well plate during the kinetic measurements, this time frame is short enough to not interfere with the test via introducing delay between wells located at different places. The microscopy image acquisition takes longer, but these images are taken only to enumerate cells before and after the kinetic measurement. Their longer time scale do not interfere with the kinetic assay that measures the repair efficiencies. **Lines 218-219**

23. Line 162-163: Similarly, the authors should also indicate how long it takes to image each well for the whole plate and if there is a significant delay between the first and last well that could influence the interpretation of repair levels between samples in the first and last wells on the plate. This would be important if a kinetics were to use a shorter time frame where differences might be amplified between samples.
The image acquisition read times were stated in the protocol. See response above and **Lines 244-248.**

24. Line 222-223: Please specify what homogenous cell count means. Same number of cells in each well? Same method/settings used for all the of the wells in the plate to get consistent normalization of the fluorescence kinetics?

We re-phrased the sentence. We meant "same number of cells per well". **Line 392-393, 669-671.**

25. Line 230: Please specify whether the fluorescence levels are normalized or not to the number of cells in each well to plot the data of the kinetics. If not, why?
Fluorescence was not normalized to the number of cells. As explained in the discussion, normalization is not possible dues to the fact that resealing efficiency varies with toxin concentration relative to cell numbers. **Lines 669-673.**

26. Line 294-295: Please Explain the importance of the difference in extinction coefficient between PI and TO-PRO-3 for this assay.
The importance of the extinction coefficient was explained. **Lines 456-458.**

27. Line 334: Figure 4C legend: Please specify which condition (M1 or M2) the images are representative of.
We specified that figure 4C, now 4A, is under M1 conditions. **Line 560-561.**